

Implantable physical sensors for in vivo organ monitoring

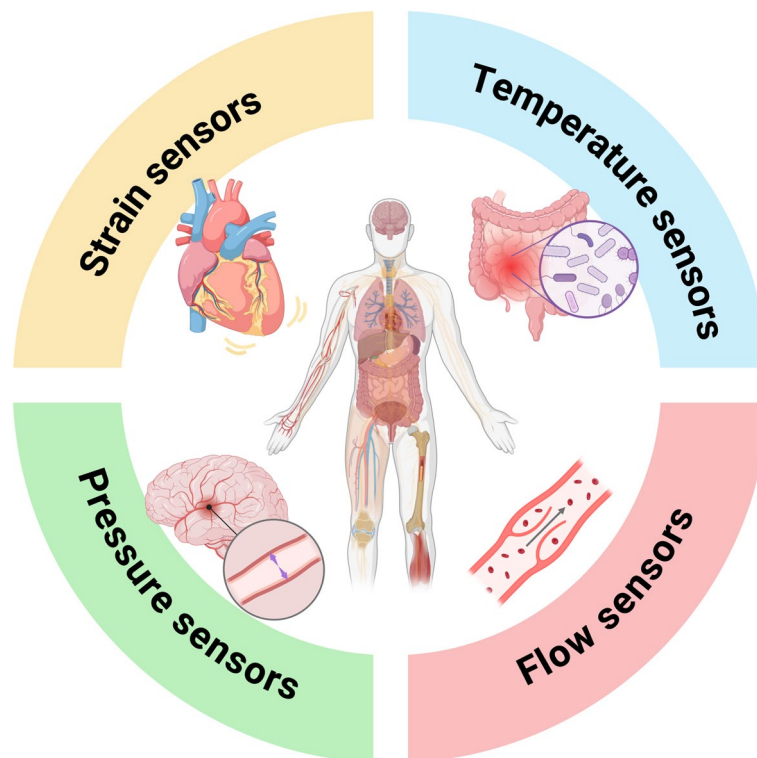
Xuan Li¹ · Xinghao Huang¹ · Liheng Yang² · Sunyoung Jung² · Jihe Wang³ · Hangbo Zhao^{1,2} 

Received: 2 September 2024 / Revised: 25 October 2024 / Accepted: 4 December 2024
© The Author(s) 2025

Abstract

Implantable sensors can provide access to accurate, continuous, and minimally invasive monitoring of physiological signals from internal organs and tissues, thereby facilitating timely diagnosis, closed-loop intervention, and advanced health management. Among the various types of implantable sensors, those capable of measuring physical parameters—such as temperature, force, and flow—are particularly important due to their ability to monitor physical conditions critical to nearly all organs and to provide insights into a wide range of health conditions. This review presents recent progress in four key types of implantable physical sensors: strain sensors, pressure sensors, temperature sensors, and flow sensors. It covers their engineering principles, design considerations, in vivo performances, and clinical relevance. The review also addresses critical challenges and future opportunities in the development of implantable physical sensors, such as flexibility and stretchability, biocompatibility, long-term stability, and the translation of these sensing technologies from bench to clinic.

Graphical Abstract



Extended author information available on the last page of the article

Published online: 08 January 2025



 Springer

Highlights

- Recent advances in implantable physical sensors are comprehensively reviewed.
- The engineering principles, design considerations, in vivo performance, and clinical applications of implantable physical sensors are discussed.
- Implantable physical sensors offer compelling opportunities for real-time, minimally invasive organ monitoring.

Keywords Implantable sensors · Physical sensors · Bioelectronics · Organ monitoring · Medical devices

Introduction

Biosensors have become integral to modern medical technologies, revolutionizing how we monitor and manage human health [1–3]. The skin, the largest organ of the body, serves as a rich source of physiological signals, leading to the development and widespread use of on-body sensor technologies—such as electronic skin, wearable devices, electronic gloves, and smart clothing [4–6]. While skin-interfaced sensors provide valuable health insights [7–10], the most critical and direct information often resides within the body's internal organs and tissues, where physiological data can be more closely correlated with specific health conditions and diseases. For instance, abnormal changes in local blood flow velocity may serve as early indicators of thrombosis, while unusual temperature fluctuations in organs can signal the onset of inflammatory diseases or organ transplant rejection [11–13]. The timely and accurate acquisition of such internal data is crucial for enhancing disease prevention, diagnosis, and treatment.

However, the skin naturally acts as a barrier, making it challenging to directly access physiological signals from internal organs and systems. To overcome this barrier, implantable sensors—including physical, chemical, and electrophysiological sensors—have emerged as a promising solution for monitoring internal physiological signals with high precision. While the field of implantable sensors is advancing rapidly, these devices face a set of complex challenges. They must account for factors such as biocompatibility, flexibility and stretchability, implantation procedures, long-term stability, and power and data transmission. Unlike skin-interfaced sensors, implantable devices must perform effectively within the body's intricate and diverse biological environments. For instance, the mechanical properties and surface structures of different organs vary significantly, necessitating customized sensor designs (Fig. 1a). The brain, with its elastic modulus of only a few kPa, requires devices with an exceptional level of softness and flexibility, in contrast with the kidney's surface, which has a modulus of hundreds of kPa [14–16]. The bladder's capacity to undergo deformation by up to 75% highlights the need for highly stretchable sensors [17, 18]. In addition, the delicate structures of nerves and blood vessels require sensors with specialized designs and implantation procedures [19, 20]. Furthermore, the long-term stability and

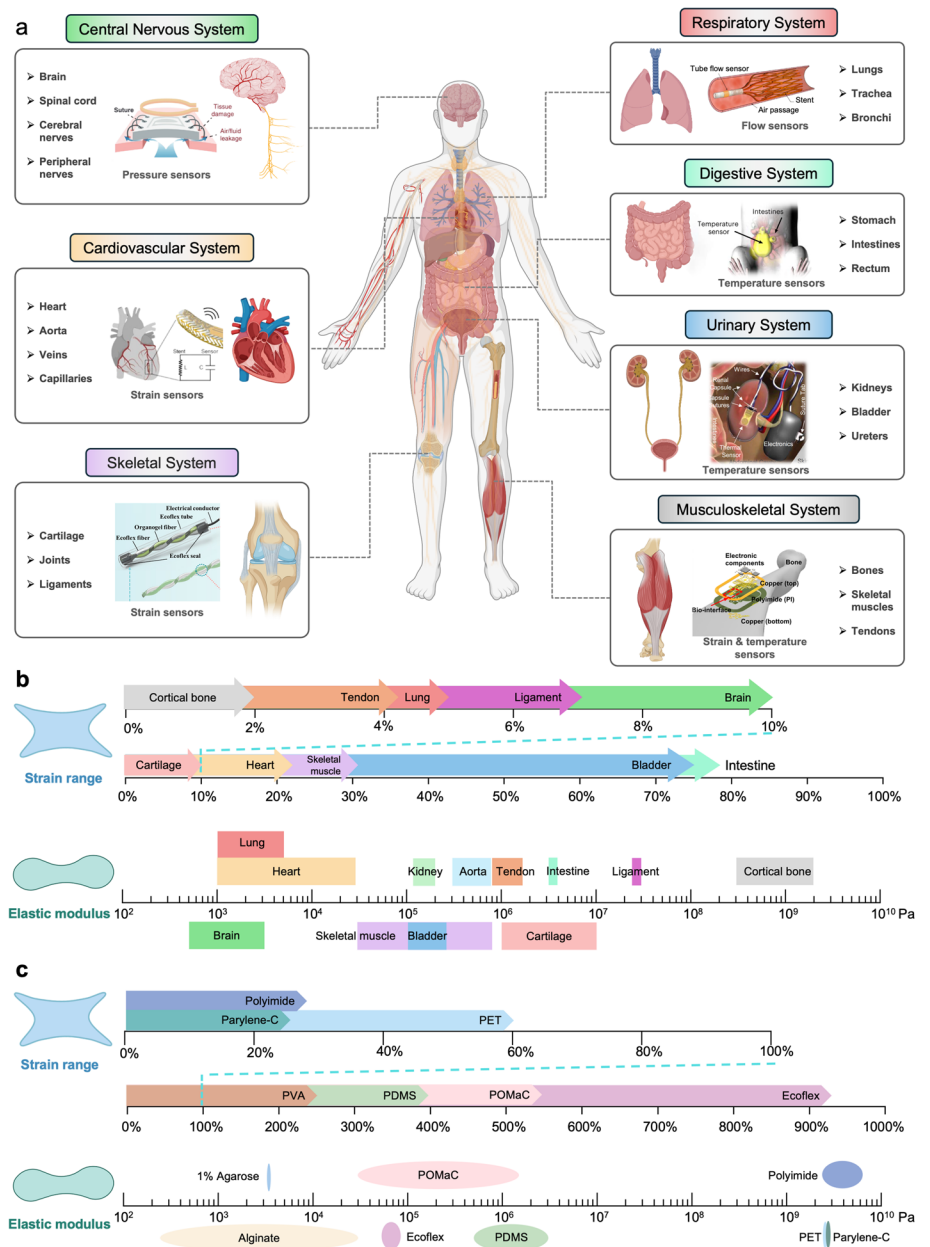
reliability of implantable sensors become even more critical when monitoring chronic and lifelong conditions, such as Crohn's disease [21, 22].

Given the diversity and complexity of the internal body environment, there remains a lack of comprehensive guidelines for designing implantable sensors tailored to specific organs and addressing the unique challenges posed by different implantation sites. In this review, we focus on implantable physical sensors, particularly strain sensors, pressure sensors, flow rate sensors, and temperature sensors. We provide an in-depth analysis of the demands for these sensors across different organs and specific diseases, reviewing the current state of these technologies and highlighting key design considerations, challenges, and future directions in this rapidly evolving field. A central focus of this review is the in vivo applications of these sensors, emphasizing how they perform within the dynamic environment of living organisms. By exploring their in vivo performances, we aim to shed light on the critical factors that influence sensor integration, functionality, and longevity in real-world clinical settings, thereby guiding future research and development efforts toward more effective and reliable solutions for organ monitoring.

Strain sensors

Strain sensors transduce deformations to electrical signals. Integrating strain sensors onto the surfaces of organs, arteries, muscles, or skeletons enables the monitoring of valuable biomechanical information to help evaluate post-surgery recovery, mitigate risks of sudden dysfunction, and assist in closed-loop control for neural modulation systems. To design implantable strain sensors for specific applications, the stiffness and strain range of the targeted organs and tissues need to be considered, as these factors are critical in determining the appropriate sensing mechanism, design, and materials [44]. Stiffness depends on both the geometry and the mechanical properties of the constituent materials. Figure 1b shows the elastic moduli and strain ranges of various organs and tissues in the human body. The elastic modulus of human tissues ranges from a few kPa in brain tissues to GPa in bones [45]. To effectively track tissue deformations with minimal constraints, implantable strain sensors should be

Fig. 1 Overview of implantable physical sensors used for health monitoring in various organs. **a** Representative examples of implantable physical sensors and their applications for organ monitoring in different systems in the body. Adapted and modified from [12, 23–28]. **b** Strain ranges and elastic moduli of different organs and tissues [14, 15, 17, 18, 28–38]. **c** Strain ranges and elastic moduli of representative substrate materials used in implantable sensors [39–43]



thin, narrow, and made from materials with an elastic modulus similar to the target tissue. Figure 1c shows the elastic moduli and strain ranges of various representative substrate materials used in strain sensors. For example, strain sensors made of soft hydrogels can be injected into brain tissues [46] or attached to the bladder [47], both of which are among the softest and most stretchable tissues in the human body. In contrast, high-modulus materials, such as polyimide (PI), are suitable for measuring micro-level strain on bones [48].

Another important factor in designing implantable strain sensors is the selection of the sensing mechanism. Commonly used strain sensing mechanisms include resistive, capacitive, electromagnetic, optical, triboelectric, and piezoelectric strain sensing [49]. Representative mechanisms are

illustrated in Fig. 2a. Electromagnetic strain sensors, such as Hall Effect Strain Transducers (HEST) or Differential Variable Reluctance Transducers (DVRT), along with traditional metal strain gauges, have been used in *in vivo* studies since the late 1990s to measure strain and force on tendons and ligaments [50]. Despite their micrometer-level resolution, these sensors are made of rigid materials that are challenging to conform to soft tissues. Optical strain sensors utilize Bragg grating [51] or light absorption [52], which rely on deformation of stretchable waveguides. These sensors provide stable strain measurements and are less sensitive to environmental factors, but they typically require expensive laser sources and measurement devices. Self-powered strain sensors based on triboelectric (TEG) and piezoelectric

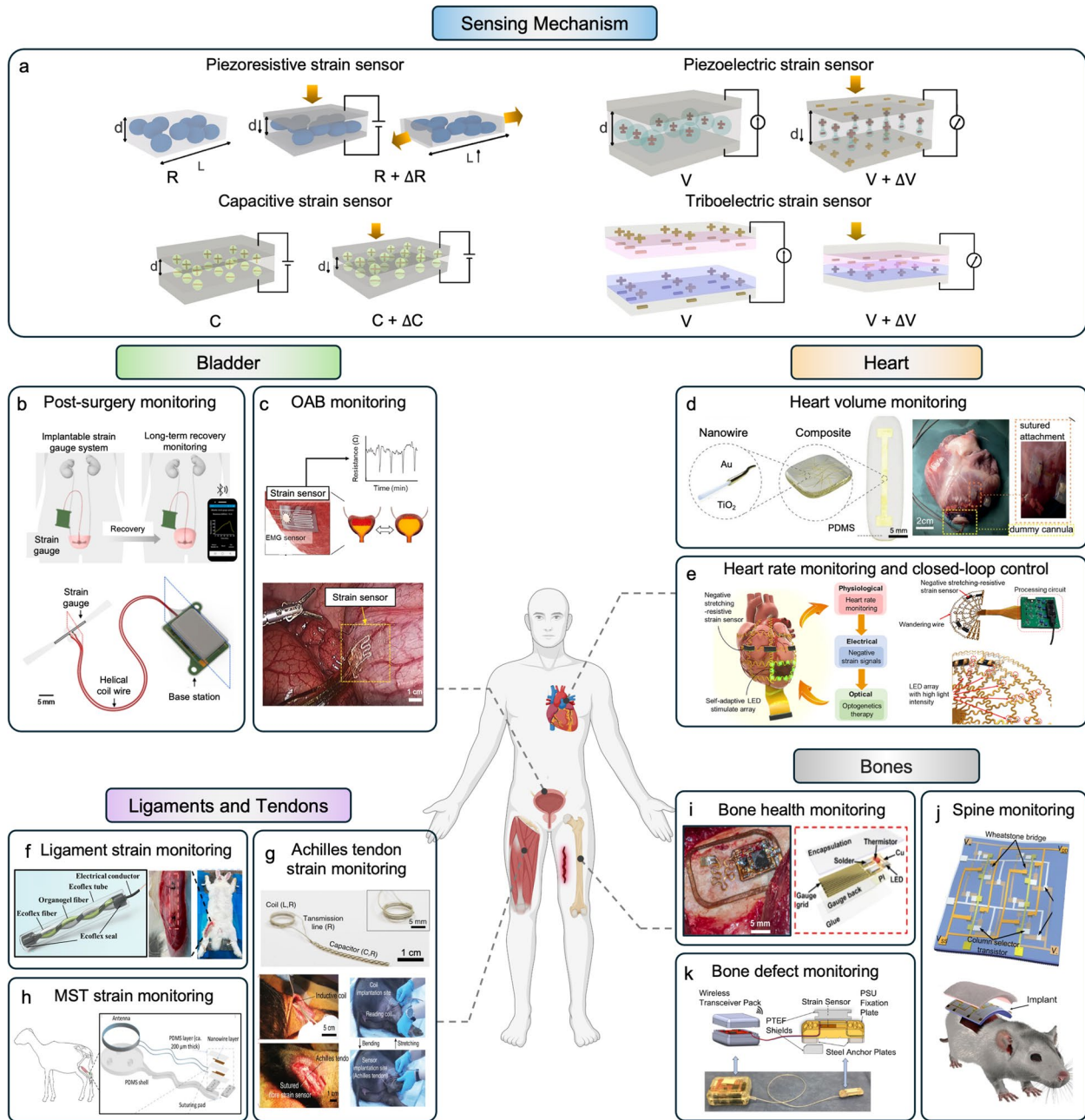


Fig. 2 Implantable strain sensors and their applications in measuring organ and tissue deformations. **a** Commonly used sensing mechanisms for implantable strain sensors. Adapted and modified from [68]. **b** A wireless strain sensing system for monitoring urinary bladder function following surgical recovery. Adapted and modified from [69]. **c** A hydrogel-based strain sensor with tissue-adhesives for monitoring overactive bladder in a pig model. Adapted and modified from [47]. **d** Fully implantable strain sensors made of Au-TiO₂ nanowires for continuous heart volume monitoring. Adapted and modified from [70]. **e** A self-adaptive cardiac optogenetics device that integrates an array of negative stretching-resistive sensors. Adapted and modified from [71]. **f** An organogel/silicone sensor for implantable ligament strain monitoring. Adapted and modified from [25]. **g** Stretchable fiber sensors for strain sensing in the Achilles tendon. Adapted and modified from [72]. **h** Schematic illustration of a strain sensor on the sheep tendon. Adapted and modified from [73]. **i** Photograph of a multimodal sensor attached to the surface of a sheep’s humerus. Adapted and modified from [27]. **j** Schematic illustration of a multiplexed strain sensing array for subcutaneous implantation in a mouse. Adapted and modified from [74]. **k** Schematic illustration of implantable strain sensors for monitoring bone defects. Adapted and modified from [75]

nanogenerators (PENGs) can harness mechanical motions to generate voltage via triboelectrification and piezoelectric effect [53]. They are effective for detecting high-frequency motions, such as finger tapping [54], heartbeats [55], or ligament stretching [25]. However, fast charge transfer within the triboelectric and piezoelectric materials makes them unsuitable for low-frequency strain sensing [56]. In contrast, resistive and capacitive strain sensors have been widely adopted in implantable devices due to their relatively high sensitivity and accuracy, ease of fabrication, and convenient signal readout. Resistive strain sensors typically utilize stretchable and fast-response sensing materials such as doped silicon [57], carbon nanotubes (CNTs) [58], MXene [59], graphene [60], liquid metals [61], and silver nanowires [62]. These sensing materials can convert deformations to large resistance changes, making them well suited for body parts that undergo small and rapid deformations. The sensor geometry and material resistivity can affect the overall sensor resistance, as described by the equation $R = \rho \frac{L}{A}$, where L , A , and ρ are the length, cross-sectional area, and resistivity of the conductor, respectively. When subjected to strain $\epsilon = \frac{\Delta L}{L}$, both the sensor geometry and resistivity can change, altering the resistance. The gauge factor (GF) can be expressed in the following way [63]:

$$GF = \frac{\Delta R/R}{\epsilon} = 1 + 2\nu + \frac{\Delta\rho/\rho}{\epsilon}, \quad (1)$$

where ν is the Poisson's ratio of the sensing material. The combined geometrical effect and piezoresistive effect can lead to high sensitivity ($GF > \sim 10\text{--}100$) and signal-to-noise ratio when the strain is small, but they may experience high hysteresis and signal drift due to irreversible changes in the morphology of the conductive sensing materials during deformation [64]. In contrast, most capacitive strain sensors rely on the strain-induced geometric changes on their electrodes and dielectric layers to detect deformations. SPoisson's ratio of the sensing material. The combined geometrical stretchable conductors such as liquid metals [65], CNTs [66], and ionic liquids [67] can maintain high conductivity for stable capacitance measurement at large strain. The capacitance of a typical parallel-plate capacitive strain sensor with length l , width w , and dielectric thickness d can be calculated using the equation $C = \frac{\epsilon_0 \epsilon_r l w}{d}$, where ϵ_0 and ϵ_r are the permittivity of free space and the dielectric constant, respectively. Capacitance under an applied strain ϵ can be expressed by the following equation (assuming the dielectric material and electrodes have the same Poisson's ratio ν for simplicity):

$$C = \frac{\epsilon_0 \epsilon_r (1 + \epsilon) l_0 (1 - \nu \epsilon) w_0}{(1 - \nu \epsilon) d_0} = (1 + \epsilon) C_0 \quad (2)$$

The resulting capacitance change is proportional to the strain, leading to a GF of 1. Other capacitive sensing structures such as interdigitated electrodes [65] or folded origami electrodes [76] can also be used to construct capacitive strain sensors. Capacitive strain sensors are generally less sensitive (i.e., smaller GF) than resistive strain sensors and more susceptible to electromagnetic interference or parasitic charges, but they can provide more stable strain measurement with lower hysteresis [49].

The following sections explore the designs and applications of implantable strain sensors for specific human tissues and organs, including the heart, bladder, blood vessels, muscles, and skeleton. We also cover material selections, implantation methods, and biocompatible encapsulation techniques for these strain sensors. Table 1 summarizes representation implantable strain sensors discussed here.

Bladder

The bladder is one of the most deformable organs in the human body. Changes in the bladder volume and pressure are closely related to its functional states. Abnormal changes in these parameters can occur due to urinary impairments, such as overactive bladder (OAB) and underactive bladder (UAB), loss of bladder sensation, or partial removal of the bladder or sphincter following surgeries [82]. Conventional bladder monitoring relies on imaging methods such as ultrasound, near-infrared spectroscopy, or magnetic resonance imaging (MRI) [82], which only provide temporary monitoring functions and require bulky, specialized equipment. Attaching implantable strain sensors on the bladder can allow continuous monitoring of surface strain that correlates to bladder volume changes. With 300%~500% volume changes in the bladder [82], strain on the bladder detrusor muscle can range from 20 to 100% [18], which requires strain sensors to be highly stretchable and durable. To address this challenge, Kim et al. have developed an implantable wireless sensing system to monitor bladder recovery after cystectomy surgeries (Fig. 2b) [69]. The system includes a strain sensor made of carbon black and silicone elastomer that can be stretched up to 300%. As the bladder expands, the sensor experiences an increase in resistance that correlates to surface strain and bladder capacity. By suturing the sensor on the bladder of a baboon, the system can successfully monitor the bladder recovery status after partial cystectomy for 8 weeks with low inflammatory responses. However, suturing strain sensors onto thin bladder walls (~ 3.4 mm thick for human [83]) can potentially damage the detrusor muscles, and open surgery may result in large incisions, increasing the risk of infection. To improve the surgical procedures and address the sensor-tissue interfacing issues, Oh et al. have developed a type of ultra-soft, hydrogel-based resistive strain sensor that can be bonded to the bladder surface (Fig. 2c) [47]. The sensor

Table 1 Summary of key parameters of representative implantable strain sensors

Implanted location	Mechanism	Main materials	Sensing performance	Ref
Bladder	Resistive	Carbon black, Ecoflex	Gauge factor: 1~5 Elastic modulus: 75 kPa Strain range: 300% Long-term stability: 8 weeks	[69]
Bladder	Resistive	Eutectic gallium-indium liquid metal, polyacrylamide hydrogel	Gauge factor: 1.1 Elastic modulus: ~1 kPa Strain range: 200% Long-term stability: 30 days	[47]
Bladder	Resistive	Silicon nanomembrane, polyimide, Ecoflex	Gauge factor: 3.3 Strain range: 60% Elastic modulus: NA Long-term stability: > 2 weeks	[77]
Bladder	Capacitive	Gold, PET, and acrylic elastomer	Gauge factor: -0.55~-3.1 Strain range: 120%	[78]
Bladder	Capacitive	Carbon nanotubes, Ecoflex	Gauge factor: 1~2.13 Strain range: 100% Elastic modulus: NA Stability: > 1 month	[79]
Heart	Resistive	Au-TiO ₂ nanowires, PDMS	Gauge factor: 5~6 Strain range: 15% Elastic modulus: ~650 kPa Long-term stability: > 7 days	[70]
Heart	Resistive	Reduced graphene oxide, PDMS	Gauge factor: 876.7 Strain range: 30% Elastic modulus: 1-3 MPa Long-term stability: > 7 days	[80]
Heart	Resistive	Graphene, PDMS	Gauge factor: > 5000 Strain range: 35% Long-term stability: 10,000 stretching cycles	[81]
Heart	Capacitive	AgNPs, polyimide, PDMS, poly(styrene-isoprene-styrene) (SIS)	Gauge factor: 12 (within 5% strain) Strain range: 16% Response time: < 200 ms (estimated) Long-term stability: 50 days (estimated)	[24]
Ligament	Triboelectric	Organogel, silicon fibers, Ecoflex	Strain range: 600% Long-term stability: 6 months	[25]
Tendon	Capacitive	AgNPs, elastomeric polyurethane fibers, PDMS, Ecoflex	Strain range: > 50% Gauge factor: 12 (at 15-27.5% strain) Long-term stability: > 40 days	[72]
Tendon	Capacitive	Au-TiO ₂ nanowires, PDMS	Gauge factor: 0.38 Strain range: 25% Resolution: 0.1% strain, ≈ 9 μm Stability: functional after 100,000 cycles of 5-20% strain and 7 days in PBS	[73]

consists of eutectic gallium-indium liquid metal printed on polyacrylamide hydrogel. By applying an anti-swelling coating, the sensor immersed in phosphate-buffered saline (PBS) after 30 days can have less than 20% weight change and minimal resistance changes. The surface functional groups of the hydrogel ($E \sim 1$ kPa) can strongly adhere to the bladder surface, and the sensor's modulus is only 1 kPa, much softer than the human bladder (~ 250 kPa [17]). The sensor is initially validated in a rat study to detect the bladder status during an induced OAB dysfunction. In a pig study, minimally invasive surgery enables the miniaturized sensor

(10 mm × 15 mm) to pass through a narrow laparoscopic tube and be directly attached to the bladder surface. The sensor then detects induced voiding and filling without constraining the bladder's deformation.

One important function of implantable strain sensors on the bladder is their integration with active neuromodulation to form a closed-loop system that controls the bladder contraction and improves urination efficiency. In this system, strain sensors usually provide feedback signals to decision algorithms, which classify bladder status and initiate electrical stimulations. In a representative study, Yan et al.

have developed a stretchable sensing and stimulation device using a CNT-based resistive strain sensor integrated into a stimulation electrode array [79]. Placing the device directly on the surface of a feline bladder and applying stimulations can simultaneously induce bladder contraction and monitor surface strain, creating a platform for potential close-loop control. Similarly, Mickle et al. have developed a closed-loop, optogenetic neuromodulation system that integrates a resistive strain sensor made of carbon black [84]. The resistance change is processed by an algorithm to identify abnormal bladder behaviors, which then activates light stimulation to trigger bladder contractions. In a more recent study, Lee et al. have developed an implantable system that consists of an electronic web for stimulation, an electronic thread for strain and electromyogram sensing, and a wirelessly powered radio frequency (RF) transmitter [77]. The system uses silicon nanomembrane as the strain-sensing element with an Ecoflex-based web structure capable of stretching up to 60% strain. To achieve closed-loop control of urination in a rat model, the system monitors strain gauge values in a detrusor underactivity model, and a decision algorithm automates electrical stimulation to induce bladder contractions. Similar closed-loop systems can also utilize capacitive strain sensors. For example, Hassani et al. have developed a platform that utilizes an interdigitated capacitive strain sensor and a shape memory alloy-based actuator [78]. In a rat study, the sensor converts bladder filling status into capacitance changes, which are used to control the actuator for voiding. Overall, the automated systems described in these studies provide real-time monitoring functions and deliver precise neuromodulation treatment for bladder dysfunction, presenting a promising method for maintaining normal bladder functions in patients.

Cardiovascular system

Cardiovascular diseases remain the leading cause of death globally. Heart muscle diseases, including myocardial ischemia or infarction, can lead to abnormal heart rhythms (arrhythmia) or stroke [85]. A key factor in assessing heart function is the myocardial strain, which refers to the contractile deformation at the longitudinal (systolic strain), circumferential, and radial directions of the ventricular chamber during each cardiac cycle, typically ranging from -17% to -23% [30]. A decrease in myocardial strain or strain rates can indicate a thickened or stiffened ventricular wall, which is closely related to hypertrophic cardiomyopathy or aortic stenosis [86]. While commonly used imaging methods, such as cardiac MRI or echocardiography, can provide 2D structural images of the heart, they are limited by the spatial resolution, frame rates, and angle dependency, and require routine patient assessment [30]. Strain sensors implanted on the heart surface offer direct and continuous measurement

of biomechanical signals such as myocardial strain, cardiac cycles, or hemodynamics. Although the strain range on the heart surface is moderate (within 20%), the ventricular volume and pressure change during one cardiac cycle only last for 0.4 to 0.7 s [87], which requires strain sensors to have high sensitivity and fast response. As a result, resistive strain sensors with high GF are typically used to monitor the heart. Recently, Dual et al. have developed a fully biocompatible strain sensor using Au-TiO₂ nanowires encapsulated by polydimethylsiloxane (PDMS) to measure heart volume changes (Fig. 2d) [70]. This type of resistive strain sensor has a gauge factor of 5 to 6 and a linear resistance change from 6 to 15% strain. The sensor maintains stable performance after immersion in 37 °C sterile Ringer solution for 7 days and over thousands of stretching cycles. In a pig study, the sensor is sutured to the epicardial wall of the pig heart and continuously monitors the volume of the left ventricle. The results indicate that the accuracy of the strain-based volume measurement is higher than the standard ultrasound echocardiography. Compared to metal nanowires, carbon nanomaterials offer even higher sensitivity to strain since tunneling is a dominant factor in their resistance change during stretching [88]. Lee et al. have developed a type of resistive strain sensor based on reduced graphene oxide and microcracked PDMS [80]. The resulting strain sensor features high sensitivity with a maximum GF of 876.7 over a range of 0% to 30% strain. To validate the functionality *in vivo*, the sensor is attached to the ventricle of a rat heart using a medical biogluce. By measuring changes in output resistance, the sensor can monitor normal and abnormal cardiac behaviors, including arrhythmia and cardiac arrest induced pharmacologically.

Strain sensors can also be integrated with other electrical components to achieve more complex therapy. For example, cardiac optogenetics is an emerging field that involves using light to control and study cardiac activities. Heart proteins are genetically modified to allow the use of light to control and stimulate different heart rhythms [89]. Hong et al. have developed a self-adaptive cardiac optogenetics device that incorporates an array of negative stretching-resistive sensors for closed-loop heart rate monitoring and light intensity control (Fig. 2e) [71]. The strain sensors are composed of CNTs and natural latex, which can have sharply decreasing resistance (75.3% reduction) at large stretching (86.6% strain). Such a negative stretching-resistive strain effect can not only be used to measure heart strain but also control the light intensity through strain-induced current change. By arranging the strain sensors and LEDs in a PI-based stretchable structure, the device is wrapped around a virus-infected beagle heart to control the heart rate by applying optical stimuli, demonstrating its effectiveness and efficiency in treating ventricular tachycardia. In addition, strain sensors combined with wireless circuits can create a fully

implantable platform that ensures continuous measurement. This design reduces infection risk and improves comfort and mobility for patients. Herbert et al. have developed a capacitive strain sensor that is integrated into an inductive antenna stent to monitor restenosis by wireless inductor-capacitor (LC) sensing [24]. This sensor design, which uses aerosol jet printing silver nanoparticles (AgNPs) and PI, forms a miniaturized parallel-plate capacitor with overlapping finger plates that can slide to change capacitance under strain. The sensor can achieve 60% capacitance change within only 5% strain, which is 10 times more sensitive than typical capacitive strain sensors [90, 91]. After implanting the sensor into heart arteries, the sensor can continuously detect the expansion and contraction induced by pulsatile flows, and the corresponding change of resonance frequency can be measured by an external antenna. In restenosis, the artery stiffens, and the sensor can detect reduced changes in capacitance and resonant frequency compared to the normal artery. However, during an accelerated aging test in saline, the sensor's baseline capacitance can almost double due to fluid penetration, which suggests the need for more effective encapsulation. Despite this limitation, wireless arterial stiffness sensing provides a robust platform for comprehensive cardiovascular health monitoring, allowing timely medical intervention and preventing severe diseases such as heart attacks and strokes.

Ligaments and tendons

Ligament and tendon injuries account for roughly 50% of musculoskeletal injuries [92]. By understanding the strain magnitude during various movements or physical activities, clinicians and researchers can better identify the mechanisms that lead to ligament injuries and tendon ruptures [93]. Due to the limited availability of *in vivo* strain measurement methods, advancements in clinical therapies for ligaments and tendons remain challenging [94, 95]. For example, HESTs and DVRTs are the only implantable sensors capable of directly measuring *in vivo* strain within human musculoskeletal tissues [50]. HESTs measure electrical potential changes caused by the relative movement between a magnet and a sensor where the electrical potential is perpendicular to both the current and the magnetic field, and it changes as the position of the magnetic field changes relative to the conductor while DVRTs detect changes in magnetic reluctance through a core moving within two coil windings [96]. A magnetically permeable core inside these coils can move within the windings [96]. These sensors provide direct, highly accurate strain measurements, are highly sensitive to detecting strains in musculoskeletal tissues, and offer high sampling frequencies [94, 96]. However, these sensors require invasive procedures [94]. Additionally, precise sensor alignment with ligament fibers is necessary, and signal artifacts can result from body movement or the sensor cable

[94]. The sensor should be capable of measuring typical tendon strains (less than 10%) while allowing the tendon to move naturally with minimal restriction [97]. To overcome these limitations, implantable strain sensors should include features such as flexibility, wireless data transmission, and enhanced stability [98, 99].

To realize real-time monitoring of ligament strain, Sheng et al. have developed self-powered and implantable strain sensors with stretchability up to 600% and stability for over six months [25]. The sensor is based on a TENG, in which organogel and silicone fibers generate charges at the interface by making contact and separating during stretching or compression. The sensor is constructed in a double helix structure and encapsulated in an Ecoflex tube. The organogel/silicon fiber-helical sensor based on TENG focuses on the dynamic strain, such as the stretching and bending motions of the ligament, facilitating injury diagnosis and rehabilitation. The sensor is tested on the patellar ligament of a male New Zealand white rabbit, where electrical signals are acquired and processed using an electrometer and acquisition card (Fig. 2f). After seven days of implantation, the sensor's electrical output remains consistent with its initial performance. This ultrastretchable, self-powered sensor system holds significant potential for continuous, real-time monitoring of ligament strain, improving the management and rehabilitation of musculoskeletal injuries.

Tendon injuries are increasingly prevalent and have become a significant health concern, often resulting from overuse or degradation due to aging [100, 101]. In current clinical practice, tissue rehabilitation is monitored through MRI or ultrasound. Implantable strain sensors can provide real-time monitoring of the mechanical properties of the healing tissues, with average tendon strains ranging from 1.1% [102] to 9.2% [103].

Lee et al. have proposed a wireless, stretchable, suturable fiber strain-sensing system designed for real-time monitoring of physiological strain in orthopedic biomedical applications [72]. The capacitive sensor comprises two highly conductive and stretchable fibers made from composites of AgNPs and elastomeric fibers. The sensor is integrated into a passive wireless RLC circuit, and an external network analyzer is used to read the sensor's data wirelessly. As the capacitance changes with strain, the resonant frequency shifts according to the formula: $f_0 = \frac{1}{2\pi\sqrt{LC}}$, where f_0 is the resonant frequency, L is the inductance, and C is the capacitance. This shift in resonant frequency allows for the wireless detection of strain without direct electrical connections. The sensor demonstrates a sensitivity of:

$$S = \frac{\delta\left(\frac{\Delta C}{C_0}\right)}{\delta\epsilon} \approx 12, \quad (3)$$

which makes it highly effective in detecting small strains (as low as 0.05%). This sensitivity is particularly important for musculoskeletal systems where tissues like tendons and ligaments undergo minor deformations. For *in vivo* testing, the sensor is implanted in the Achilles tendon of a miniature pig, and its wireless functionality and stability are demonstrated over a period of three weeks (Fig. 2g). The observed strain change is approximately 3.09%, which is within the expected physiological range for the Achilles tendon. The sensor is biocompatible, as confirmed by cell viability tests with human cardiac microvascular endothelial cells. Its design, high sensitivity, and wireless capabilities make it a promising tool for biomedical applications, including personalized rehabilitation and continuous monitoring of musculoskeletal conditions.

A strain sensor with low stretchability can potentially damage nearby musculoskeletal soft tissues (MSTs), while poor fixation during MST strain measurements and the use of wired sensors can lead to artifact signals when the sensor bends [104]. Similar to cardiac muscles, MST strain measurements benefit from wireless, stretchable sensors for monitoring the health and function of ligament and tendon tissues that are responsible for movement, stability, circulation, and overall bodily function [105]. However, extreme motions make these muscles easily damaged and have limited ability to regenerate [106]. Given the challenges of repairing injured muscle tissues, implantable strain sensors are valuable for real-time monitoring and measuring muscle strain with flexibility. Zhang et al. have proposed a stretchable capacitive strain sensor integrated with an inductor to form an LCR circuit that enables wireless strain measurements through resonant frequency changes [73]. Its stretchable feature allows the sensor to endure the deformation of the MSTs and offers a higher resolution for strain measurement with a wireless readout box. The sensor consists of conductive gold-coated titanium dioxide nanowires embedded in a dielectric silicone rubber layer to form a “sandwich” structure, and the capacitor is bonded to a coil inductor to form the LCR circuit that is encapsulated with PDMS (Fig. 2h). As the sensor is stretched, the capacitance changes due to dielectric layer deformation and variations in the overlapping area of conductive layers. The sensor exhibits excellent resolution (0.1% strain, $\approx 9 \mu\text{m}$) and maintains high linearity ($R^2 > 0.99$) for strains between 0 and 25%. Additionally, the sensor retains the linearity and resolution of the capacity over 100,000 cycles of fatigue loading. *Ex vivo* tests on sheep tendons show reliable strain measurement, with an average strain of 4.2%, whereas *in vivo* tests demonstrate successful dynamic strain measurement during locomotion. The sensor is first pre-stretched by 15%, and then it is sutured to the medial gastrocnemius tendon of a sheep. The sensor system can be used to quantify musculoskeletal soft tissue strains during functional activities, providing insights

into tissue biomechanics, pathology, and adaptation during healing.

Bones

Bone is a dynamic tissue that undergoes continuous remodeling and, following injuries, possesses the capacity to regenerate, restoring its biological and mechanical properties to their pre-injury condition [107]. The creation of a continuous monitoring technique to evaluate adequate bone loading during rehabilitation can enhance patient quality of life [108]. Implantable strain sensors for bones can provide continuous insights into tissue strain during rehabilitation protocols and daily activities, enabling adjustments to be made based on the tissue's tolerance levels [97]. Strain levels and strain rates are the key parameters for evaluating the biomechanical properties of soft tissues and assessing their healing progress [97]. The reported ranges for strain accuracy and precision in the literature are 20 to $\sim 1,280 \mu\epsilon$ for accuracy and 39 to $\sim 630 \mu\epsilon$ for precision [109]. Cai et al. have introduced wireless, battery-free, and multimodal biointerfaces, known as osseosurface electronics, for monitoring the musculoskeletal system, diagnosing bone health, and providing therapeutic stimulation in freely moving animal models [27]. The device is designed for direct application to bone surfaces, opening new possibilities for long-term monitoring and therapeutic applications in musculoskeletal health. Osseosurface electronics are ultra-thin, wireless, and battery-free, allowing for real-time recording of physiological and biophysical signals such as bone strain, temperature, and optoelectrical stimulation. The primary sensor is a metal-foil strain gauge laminated onto the bone surface. The system utilizes Near Field Communication (NFC) for wireless powering and data transmission. The wireless osseosurface electronics system is implanted into rats, and a cyanoacrylate-based adhesive is used to bond the strain gauge and other components directly to the bone surface (Fig. 2i). *In vivo* strain measurements are performed during gait analysis, with strain values ranging from 0 to $1200 \mu\epsilon$ during typical gait cycles. After two weeks of implantation, the device becomes surrounded by fibrous tissue, indicating successful tissue integration. Surface-engineered calcium phosphate ceramic particles are used to facilitate the integration of the electronics with the bone, enabling stable, long-term monitoring. In addition to small animal testing, the system is also tested in sheep models. These tests validate the device's scalability and demonstrate that the sensors reliably capture bone strain through thicker tissues (up to 11.5 cm deep).

Bone fractures are a global public health concern, especially in individuals with osteoporosis, as they can result in disability and higher healthcare costs, placing a significant burden on both individuals and healthcare systems [110]. Spinal cord injury is a serious medical issue causing severe

disability and high mortality [111]. Therefore, real-time continuous monitoring of spinal or joint movements can optimize patient rehabilitation, reducing the likelihood of requiring a second surgery [112]. Orthopedic implants are one example solution to achieve this, and they are designed to handle mechanical demands, including load-bearing strength and elasticity for withstanding shear stress [113]. Zhang et al. have presented a dual-functional smart coating foil that can be applied to commercial orthopedic implants to address key challenges in orthopedic implants, such as infections and implant failures [74]. A multiplexed strain-sensing array based on single-crystalline, piezoresistive silicon nanomembranes. The strain-sensing array, made of multiple single-crystalline silicon strain gauges, is distributed across the implant's surface to provide high-resolution, real-time mapping of strain in different regions (Fig. 2j). The strain-sensing functionality of the coating is tested in an ex vivo sheep spinal fusion model. After destabilizing the spine, the strain on the spinal rod increases by $0.04 \pm 0.01\%$, suggesting that more load is transferred to the rod due to reduced vertebral stiffness. When bone cement is used to restore stiffness, the strain decreases by $0.06 \pm 0.02\%$, confirming that the coating's sensors can detect strain changes during the fusion process.

Mechanical forces and properties play a crucial role in guiding tissue repair, as well as regulating stem cell function, and developmental processes [114]. Moreover, mechanical loading can enhance the quantity and functionality of regenerated bone, particularly when this bone is generated through endochondral ossification. Additionally, muscle-exerted mechanical forces play significant roles in skeletogenesis [115, 116]. Strain sensors can be effective tools for advancing our understanding of bone mechanics and improving the outcomes of orthopedic treatments and rehabilitation programs. Klosterhoff et al. have proposed a wireless, implantable strain sensor designed for real-time monitoring of mechanical boundary conditions across bone defects [117]. The strain sensor is designed to measure strain across a bone defect longitudinally during rehabilitation (Fig. 2k) [75]. The platform integrates the strain sensor into the polymeric bridging segments of internal fixation plates. For real-time monitoring of mechanical boundary conditions, two types of internal fixators are used—stiff polysulfone (PSU) fixators and compliant Ultra-High Molecular Weight Polyethylene (UHMWPE) fixators—to create different mechanical environments. The UHMWPE fixators double the strain magnitude compared to PSU, initially averaging 5408 ± 704 microstrain ($\mu\epsilon$) and decreases to 2698 ± 567 $\mu\epsilon$ as the bone defect heals, reducing the load carried by the fixator. The UHMWPE group experiences compressive strain of 0.1% to 6.7%, while PSU fixators show lower strains of 0.1% to 0.9%. The wider range of tissue

strain in the compliant fixation group shows that the tissue is exposed to more varied forces, which facilitates healing. Increased mechanical stimulation improves early bone formation and healing. These results suggest that strain monitoring can offer a non-invasive way to assess bone repair, potentially reducing the need for X-ray imaging.

Pressure sensors

Pressure sensors convert pressures exerted on tissues to electrical signals and they can be used for detecting fluid pressure or volumetric changes of targeted organs, such as the brain, eyes, arterials, and bladder. Pressure sensors can be applied during surgery, shortly after surgery, or for various diagnostic purposes, including intracranial, arterial, and urinary bladder pressure monitoring. The form factor, pressure range, and measurement sensitivity are some of the key criteria for an implantable pressure sensor, which should be tailored for targeted organs.

Pressure sensing mechanisms mainly include capacitive (Fig. 3a), piezoresistive (Fig. 3b), and optical fiber detection (Fig. 3c). The sensing mechanism determines the structure and configuration of a pressure sensor. For instance, a spherical capacitive pressure sensor detects arterial circumference changes through capacitance variations [118]. A piezoresistive pressure sensor detects diaphragm bending as a change in resistance within the piezo resistors embedded in the diaphragm [119]. In fiber optic catheters, pressure sensors placed at the tip convert wavelength changes into pressure readings [120]. Implantable pressure sensors are particularly useful for measuring intravascular blood pressure, intracranial pressure, and intraocular pressure.

A major obstacle to long-term pressure sensing in the human body is biofouling on the pressure-sensitive region of the sensor. The human immune response can be dynamic, resulting in varying thicknesses of the layers accumulating on the sensor's surface, affecting the sensor readings. Additionally, corrosion of sensor materials by body fluids can lead to sensor failure.

Innovations such as bioresorbable materials and wireless transmission technologies further enhance the utility and safety of these sensors by reducing infection risks and improving patient compliance [74, 122, 127]. Continuous data streaming provided by these sensors reduces the need for repeated surgeries, thereby minimizing infection risks and improving patient outcomes and healthcare efficiency. The following sections highlight recent advances in implantable pressure sensors used in the central nervous and cardiovascular systems, with representative examples summarized in Table 2.

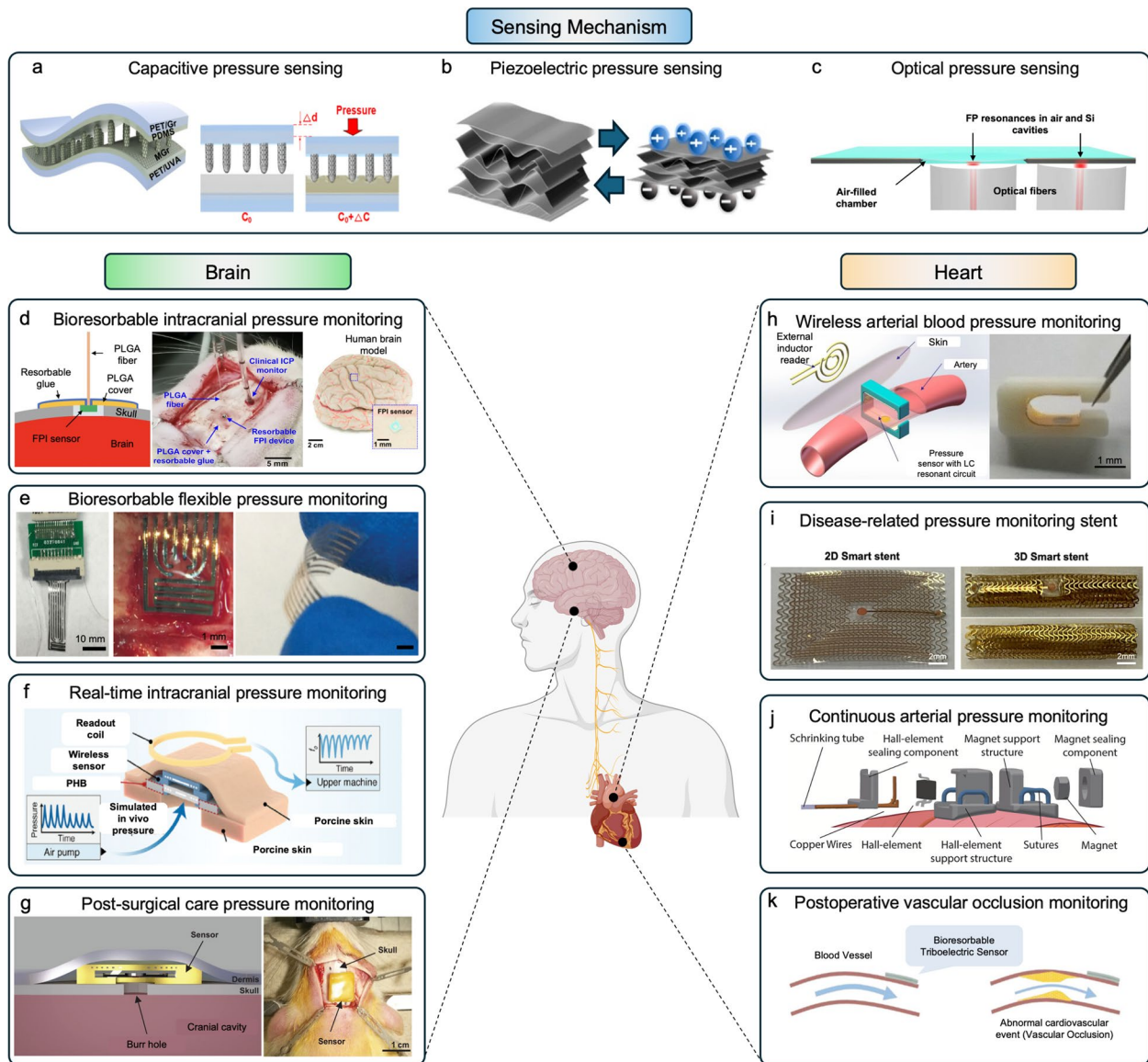


Fig. 3 Implantable pressure sensors and their applications in measuring intracranial pressure, blood pressure, and other internal pressures. **a** A schematic illustration of a capacitance pressure sensor. Adapted and modified from [118] **b** Schematic illustration of a piezoelectric pressure sensor. Adapted and modified from [119] **c** Schematic illustration of an optical pressure sensor. Adapted and modified from [120]. **d** A bioreabsorbable optical sensor that converts wavelength to pressure for monitoring the intracranial pressure. Adapted and modified from [120]. **e** An LC circuit-based resistive pressure sensor that converts deformation in serpentine Mo track to pressure for monitoring intracranial pressure. Adapted and modified from [121]. **f** Schematic illustration of a bioreabsorbable wireless resistive pressure sensor with hydrogel bioadhesive. Adapted and modified from [23]. **g** A bioreabsorbable, piezoelectric pressure sensor that translates electrode deformation to pressure for post-surgical care. Adapted and modified from [122]. **h** A wireless ex-arterial cuff-like capacitive sensor located on the aorta and encapsulated with PDMS and PI. Adapted and modified from [123]. **i** A thermally self-reporting capacitive polymer stent that converts change in capacitance to pressure for detecting in-stent restenosis and cardiac functional dynamics. Adapted and modified from [124]. **j** An extra-arterial Hall-based magnetic sensor for continuous monitoring of blood pressure and vascular hemodynamics. Adapted and modified from [125]. **k** A bioreabsorbable triboelectric pressure sensor that converts voltage changes to pressure for continuous cardiovascular postoperative monitoring. Adapted and modified from [126]

Brain

Brain-implantable pressure sensors hold substantial clinical significance and have proven to be especially applicable for measuring real-time intracranial pressure (ICP) [128, 129]. In the central nervous system, ICP-induced brain

damage is a significant health and socioeconomic challenge worldwide [122]. Real-time ICP monitoring is crucial for managing conditions such as traumatic brain injury [128], hydrocephalus [130], and other neurosurgical conditions [131]. ICP is assessed through pressures in closed compartments and lumina within the body to diagnose conditions

Table 2 Summary of key parameters of representative implantable pressure sensors

Implanted location	Mechanism	Main materials	Sensing performance	Ref
Calvaria	Optical fiber	Silicon dioxide, amorphous silica	Range: 0—15 mmHg Sensitivity: 3.1 nm/mmHg Long-term stability: 25 days	[120]
Calvaria	Resistive	PLGA, PLLA/PCL, molybdenum	Range: 0—75 mmHg Long-term stability: 5 days	[121]
Calvaria	Capacitive	Poly(HEMA-NVP) + Poly(AA-NHS), PLGA, POC, magnesium	Range: 0—40 mmHg Sensitivity: 1 MHz/mmHg Long-term stability: 50 min	[24]
Calvaria	Capacitive	Si ₃ N ₄ , Zinc, PLGA, magnesium, natural wax	Range: 0—15 mmHg Resolution: 1 mmHg Sensitivity: 200 kHz/mmHg Long-term stability: 4 days	[122]
Extra-arterial	Resonance frequency shifts	PDMS, polyimide, chromium, gold	Range: 80—120 mmHg Sensitivity: 8.53 kHz/mmHg Long-term stability: 5 days	[123]
Extra-arterial	Halls effect	Parylene-C, biocompatible resin DS300, epoxy	Range: 30—220 mmHg Sensitivity: 45 mv/mt Long-term stability: 7 days	[125]
Extra-arterial	Piezoresistive	PLA/C, magnesium, POC	Range: 0—170 mmHg Sensitivity: 11 mV/mmHg Long-term stability: 5 days	[126]
Intra-arterial	Piezoresistive	SU-2002, SU-3010, SiO ₂ , titanium, copper, PermiNex, silicon	Range: 0—300 mmHg Sensitivity: 3.5 kHz/mmHg	[124]

such as ischemia [132], intra-abdominal hypertension [133], and pulmonary hypertension [122]. Fluctuations in ICP are driven by changes in the circulatory dynamics of cerebral blood and cerebrospinal fluid [134]. The normal range of ICP is from 7 to 15 mmHg [135]. Physiologically, a 5 to 10 mmHg increase in ICP can obstruct blood flow [136], leading to life-threatening ischemia [137]. Intra-abdominal hypertension is characterized by an ICP higher than 12 mmHg [138], contributing to morbidity in critically ill patients. An ICP above the 20 mmHg threshold requires immediate medical attention; and a pulmonary artery pressure over 25 mmHg is associated with various heart and lung conditions [24, 120, 122, 139]. Elevated ICP is a hallmark of secondary brain injury, demonstrating the critical need for real-time monitoring to prevent further complications. Continuous real-time detection of ICP through implantable pressure sensors significantly aids the monitoring of these conditions [120, 130]. Therefore, a successful implantable pressure sensor for the brain should demonstrate sufficient sensitivity within 5 mmHg to achieve maximum clinical outcome. ICP pressure sensors access the intracranial space to detect pressure through a small craniectomy defect drilled at the top of skull, avoiding direct contact with the brain to minimize immune responses.

Different types of bioresorbable implantable pressure sensors—optical [120], capacitive [121], resistive [24], and piezoelectric [122]—demonstrate excellent ICP detection capabilities while offering a promising solution to reduce

the risks of infection and immune response. In addition to reducing the need for surgical extraction of the sensors, the increased lifespan of these bioresorbable implantable sensors enables more measurements compared to the non-resorbable, commercial devices with biodegradability and minimal biological impact [120]. Figure 3d highlights a miniaturized, tri-layer piezoelectric sensor developed by Shin et al. [120], which consists of a thermally grown ultrathin silicon wafer (t-SiO₂), a silicon nanomembrane, and a silicon slab with cavity. The pressure-sensitive diaphragm exhibits a piezoresistive response in the strain gauge that depends on the mechanical equilibrium between the pressure of the surroundings and that of the air trapped inside the cavity [120]. In this configuration, the thickness of the diaphragm is inversely proportional to the wavelength detected by the PLGA optical fiber, which translates into the ICP. The t-SiO₂ acts as a barrier to protect the underlying silicon nanomembrane (~200 nm) used as an adhesive layer for both silicon and silicon dioxide, and a buried SiO₂ layer (~600 nm) provides electrical insulation and mechanical support. The sensor is encapsulated with a 100- μ m-thick bioresorbable polyanhydride layer to protect the sensor-wire interface from biofluid exposure. In the rat model *in vivo* test, the sensor is placed intracranially through a craniectomy defect and sealed with bioresorbable glue. Additionally, the sensor is capable of both wired and wireless data transmission via a miniaturized wireless potentiostat [120]. The pressure sensor developed by Shin et al. combines the fiber optic and

piezoelectric sensing mechanism to detect ICP, demonstrating stable sensitivity within the range of 3 mmHg to 15 mmHg for up to 25 days during the rat in vivo test.

Xu et al. have proposed PLLA/PCL (80:20) for pressure sensor encapsulation to overcome the elastic modulus mismatch compared to other encapsulation substrate materials. Their flexible, bioresorbable electrocorticography (ECoG) device is made of materials that improve biocompatibility and reduce infection risks associated with device removal, while integrating ICP monitoring for comprehensive brain health assessment. The bioresorbable ECoG device with an integrated ICP sensor features a serpentine molybdenum (Mo) track deposited on a poly(L-lactide) PLLA/PCL (80:20) substrate with a total thickness of 40 μm . As the Mo track experiences deformation, it exhibits a measurable change in the electrical resistance that linearly correlates with pressure [121]. In the in vivo animal test, pressure readings obtained from rats confirm the linear relationship between resistance and pressure. The sensor functions effectively for five days within its ICP monitoring range from 0 to 75 mmHg, with the sensor fully degraded in approximately 100 days [121] (Fig. 3e). Although the pressure sensor utilizes PLLA/PCL to reduce elastic modulus mismatch and demonstrates stability through the rat in vivo test, the pressure sensor's thickness still triggers immune responses in the brain.

Recent advances in electronics-tissue bio-interface technologies have enabled the development of highly reliable and biocompatible sensors for long-term disease diagnosis and treatment. A key challenge has been achieving robust anchorage of pressure-sensing bioelectronics onto dynamic biological tissues. In this implantable flexible pressure sensor, LC magnesium coils are encapsulated in poly(lactic-co-glycolic acid) (PLGA) film. PLGA film also serves as the dielectric layer in this sensor design [24] (Fig. 3f). Structurally, a poly(1,8-octanediol-co-citrate) (POC) layer supports the capacitor, while a poly(HEMA-NVP) hydrogel substrate and poly(AA-NHS) polymer brushes form the adhesive bio-interface. The resonance frequency is crucial for the sensor's operation as it detects changes in pressure through frequency shifts. In an in vivo rat model test, the sensor is successfully implanted through a skull hole and adhered using a hydrogel bio-adhesive to enable real-time ICP monitoring for up to five hours [24]. However, further investigations are needed in dynamic environments and long-term settings. Another bioresorbable pressure sensor that also operates on passive LC resonance circuits achieves a sensitivity of approximately 200 kHz per mmHg and a resolution as low as 1 mmHg [122] (Fig. 3g). Moreover, this bioresorbable pressure sensor utilizes natural wax and Si_3N_4 for encapsulation, allowing the sensor to maintain functionality for four days without adverse reactions [122].

Heart

Cardiovascular coronary artery diseases (CADs) are prevalent and carry a high mortality rate, accounting for more than 17 million deaths around the world annually, according to the World Health Organization [140]. Implantable pressure sensors enable real-time cardiac monitoring through continuous measurement of blood pressure via either a close interface or an incision with the heart and artery. CAD is primarily caused by atherosclerosis, a condition in which plaque builds up inside the coronary arteries. Plaque consists of fat, cholesterol, calcium, and other substances found in the blood. Over time, this buildup can harden or rupture, leading to the narrowing or blockage of the arteries. Cardiovascular conditions such as heart failure, stroke, peripheral arterial disease, and hypertension contribute to potential cardiac arrest, angina, dyspnea, and heart attacks due to blockages that impair the transfer of blood to the heart. In cardiovascular applications, implantable pressure sensors play a crucial role in monitoring conditions such as CAD [141], heart failure [142], and hypertension [122]. These pressure sensors enable close monitoring of blood pressure and flow dynamics within the heart and major blood vessels [143], allowing for early detection and management of cardiac events. A successful heart pressure sensor offers precise monitoring while providing the patient with a clear arterial pathway. Extra-arterial placement [123, 124, 126] and the use of stent-like structures [125] for cardiac pressure sensor can achieve both objectives.

Implantable pressure sensors in or near the cardiovascular system utilize the circumference changes to measure either the capacitance changes between two parallel plates [123, 124] or the distance changes between two sensing magnets [125]. Besides utilizing the difference in distances, ambient pressures can also be converted into electrical signals [126]. Figure 3h presents a wireless passive extra-arterial implantable blood pressure monitoring sensing system, operating based on an LC resonant circuit [123]. The system consists of an extra-arterial miniature-sized cuff style parallel-plate capacitor and an external planar spiral inductor, where pressure changes within the artery cause the flexible diaphragm constructed with chromium and gold to deform, changing its capacitance and the resonant frequency of the LC circuit. The resonant frequency shift is detected by an external read-out coil (f) through electromagnetic coupling, which allows wireless measurement of the blood pressure. Additionally, the sensor utilizes adaptive radio frequency powering for wireless transmission, reducing the size and potential complications associated with battery replacement. The sensor, encapsulated with biocompatible PDMS and polyimide, has a maximum detection distance of 22 mm between the two parallel plates, and the external coil is connected with the impedance analyzer. The accuracy of the sensor is verified

by comparing its readings with those of commercial pressure sensors in an *in vivo* environment for up to five days with a difference of less than 5%, which can be numerically compensated for improved accuracy [123].

To overcome the limitations in sensitivity and data collection issues, a self-reporting stent with an inductor coil-encapsulated pressure sensor for monitoring arteries blood pressure internally has been developed [124]. This innovation enables validation through comprehensive testing that demonstrates high sensitivity and reliability. The sensor uses titanium and chromium for its sensing area and employs SU-2002, SU-3010 and PermiNex for encapsulation [124] (Fig. 3i). This construction increases the sensing resolution and coupling distance between the sensor and the external antenna. After self-assembly due to thermal bonding and precise alignment of the capacitor plates and inductor coils, the dual-pressure sensors enable the detection of blood flow *in situ*. The stent is crimped onto a balloon catheter, which is later inserted into the target artery. Furthermore, the stent's structure is designed to maintain its position and provide necessary mechanical support to the artery. The stent converts the deformation of polymer to resistance. During the *in vivo* test, the self-reporting stent is implanted into the rat's femoral artery and monitored wirelessly using a vector network analyzer (VNA) externally [124]. The stent is designed to be implanted within blood vessels, particularly targeting sites with a high risk of restenosis.

In addition to the novel stent design, another innovative approach has emerged for cardiovascular monitoring. A sensor that utilizes a Hall-based magnetic flux mechanism to monitor arterial blood pressure, arterial diameter, and arterial circumferential strain continuously has been developed [125] (Fig. 3j). This design, validated both *in vitro* and *in vivo*, provides accurate and detailed cardiovascular monitoring under various physiological and pathological conditions, offering potential for improving patient compliance surveillance and treatment management in cardiovascular diseases. The sensor comprises a Hall-effect sensor and a miniature magnet attached to the outer wall of the aorta without physical interconnection, thereby avoiding vascular restriction and material fatigue (Fig. 3j). The heart's pulsatile actions alter the distance between the HES and the magnet, changing the magnetic flux and generating a corresponding voltage output to calculate arterial diameter, circumferential strain, and blood pressure. The arterial pressure can be expressed as

$$P = \frac{\delta}{R} \left(\epsilon \cdot \epsilon_{\zeta} + R_m \cdot \frac{d\epsilon_{\zeta}}{dt} \right), \quad (4)$$

where δ is the thickness of the arterial wall, R is the arterial wall radius, ϵ is the elastic Young's modulus, ϵ_{ζ} is the circumferential arterial strain, and R_m is the viscoelastic modulus. The sensor's components are encapsulated in

3D-printed biocompatible resin and coated with parylene-C for enhanced durability [125]. Surgical implantation involves suturing the components to the aorta, verified by fluoroscopy for precise alignment. In porcine model tests, the sensor demonstrates a mean absolute error below 5 mmHg for blood pressure measurements, and the readings remain stable under varying conditions for up to seven days.

A recently reported bioresorbable implantable pressure sensor uses triboelectric principles [126] (Fig. 3k). This bioresorbable dynamic pressure sensor (BTS) is designed for monitoring cardiovascular functions post-surgery by providing real-time data on blood pressure and vascular health. The air spacer structure in the triboelectric sensor ensures that the separation of triboelectric layers is governed by the air, aligning the device's mechanical properties with the ideal gas law. This design results in a linear relationship between pressure changes and the open-circuit voltage output:

$$\Delta P = \frac{nRT\epsilon_0 U_{oc}}{x_0 \sigma}, \quad (5)$$

where ΔP is the pressure change, n is the number of moles, R is the universal gas constant, T is the temperature, ϵ_0 is the permittivity of the vacuum, x_0 is the initial displacement, σ is the surface charge density, and U_{oc} is the open-circuit voltage. Constructed primarily from magnesium and encapsulated in biocompatible materials such as gelatin methacrylate and PLA/C, the BTS can be minimally and invasively attached to the vascular wall or placed under the skin [126]. In *in vivo* animal tests in rat and dog models, the sensors exhibit high sensitivity to pressure changes with a linear relationship between pressure and output voltage. Although the encapsulation layer begins to degrade after five days, the BTS demonstrates good biocompatibility with no significant inflammatory reactions over nine weeks. Furthermore, the sensor's performance and degradation are evaluated in rat and beagle dog models, and the sensor completely degrades after 12 weeks [126]. The sensor helps detect abnormal cardiovascular and respiratory events, such as arrhythmias and vascular occlusions, facilitating early intervention and potentially preventing severe complications. Its bioresorbable nature eliminates the need for follow-up removal procedures, reducing healthcare costs and burdens.

Aside from the central nervous system and cardiovascular system, implantable pressure sensors also demonstrate promising functionalities for other physiological systems, including respiratory monitoring and chronic condition management [120]. The implantable *in vivo* sensor's ability to provide high-accuracy, real-time pressure measurements strengthen medical personnel's clinical decision-making and enhance patient care. In addition to the significant clinical benefits, ongoing challenges include extending the operational lifetime and ensuring the encapsulation integrity of these sensors. Overall, implantable flexible pressure sensors

represent an important advancement in biomedical technology integration, providing a robust alternative for continuous internal pressure monitoring across various organ systems [98].

Implantable pressure sensors not only provide real-time, stable, and quantitative measurements for the central nervous system and circulatory system, but they can also be applied to the respiratory system and other physiological systems and applications. These implantable devices are intended for long-term monitoring of chronic conditions in patients with brain injuries or diseases, eliminating the need for surgical removal and reducing infection risk, healthcare costs, and patient distress. When a patient's ICP requires repeated or continuous measurement, the implantable pressure sensors provide a minimally invasive alternative without repeated surgical interventions. At the same time, as the implantable pressure sensor's operational lifetime is extended, the need to replace the sensor is reduced, which further decreases the chance of critically ill patients undergoing additional surgeries and being exposed to infections. Their high accuracy in pressure measurement supports better clinical decision-making and improved patient outcomes. Although these sensors demonstrate significant clinical benefits, challenges remain in extending their operational lifetime.

Flow sensors

Blood flow velocity is a critical physiological parameter that varies widely across different vascular systems and states of health [144]. Implantable flow sensors are crucial for diagnosing and monitoring vascular diseases such as aneurysms, atherosclerosis, and thrombosis, which can cause vessel wall damage and inflammation, potentially leading to fatal outcomes [145, 146]. Moreover, continuous hemodynamic monitoring is important to measure critical hemodynamic parameters such as blood pressure, heart rate, and temperature via real-time data transmission [147, 148], which can significantly improve patient care, offer early detection, and detect adverse events in a timely manner. Traditional respiration monitoring devices tend to have limitations, including bulkiness, and high costs, making them unsuitable for daily use [149]. As a result, there has been a growing focus on developing more attractive methods for user-friendly respiration monitoring [149]. The breathing rate is a crucial vital sign in human physiology, providing valuable insights into an individual's overall well-being [150]. In addition to blood flow sensing, sensors capable of real-time breathing monitoring have the potential to serve as valuable diagnostic and monitoring tools for respiratory conditions, including asthma, and sleep apnea [150]. Self-powered respiration sensors are attracting interest because they can convert the energy from breathing, such as biomechanical or thermal

energy, into electricity. Technologies such as triboelectric, piezoelectric, pyroelectric, and electromagnetic nanogenerators make these sensors portable with low-maintenance [149]. Examples of self-powered respiration sensor systems are triboelectric, piezoelectric, pyroelectric, hygroelectric, electromagnetic, and hybrid [149]. Figure 4 a-d illustrate the mechanisms of TENG, PENG, pyroelectric effect, and hygroelectric effect. TENG can operate in four main modes: the vertical contact-separation mode generates electron flow by periodic contact and separation of two triboelectric layers with different electron affinities; the lateral sliding mode can capture energy from different directions but may compromise durability; the single-electrode mode features one movable electrode while the other is grounded; the freestanding mode has two electrodes remain stable, connected through a load, and charge transfer is induced by a moving dielectric segment. The PENG involves disrupting the central symmetry of the crystal structure in piezoelectric materials through the application of external force. Pyroelectric materials generate an electrical charge when their temperature changes. This occurs due to shifts in their internal dipole alignment, which alters the surface charge and creates an electric current. The hygroelectric effect converts the potential energy of water molecules directly into electrical energy. Detailed discussions of different types of flow sensors used in various target organs appear in the following sections and are summarized in Table 3.

Cardiovascular system

Figure 4e presents implantable flow sensors developed by Kwon et al., which is a batteryless wireless vascular flow rate sensor powered by a Bluetooth low energy (BLE) system-on-a-chip [151]. The sensor integrates pressure, flow, and temperature sensing, with a strain sensor that features a buckled bending cantilever to measure both forward and backward arterial flow rates. The sensing module consists of strain gauges made from thin monocrystalline Si-NMs to measure blood flow, pressure, and temperature. The sensor operates based on the piezoresistive effect, utilizing a bi-directional flow sensor with a 3D curvy ribbon. Forward and backward blood flows deform this 3D structure, inducing tensile and compressive strain in the Si-NMs, resulting in corresponding resistance changes:

$$\Delta R(\%) = GF \times \epsilon \quad (6)$$

For Si-NM strain gauges under forward and backward flow, the GF values range from 30 to 100. Additionally, the system includes a wireless electronics module that interfaces with the sensing module. It uses a receiver coil resonant at the NFC frequency (13.56 MHz) and transmits data wirelessly via BLE protocols. A porcine model evaluates sensor

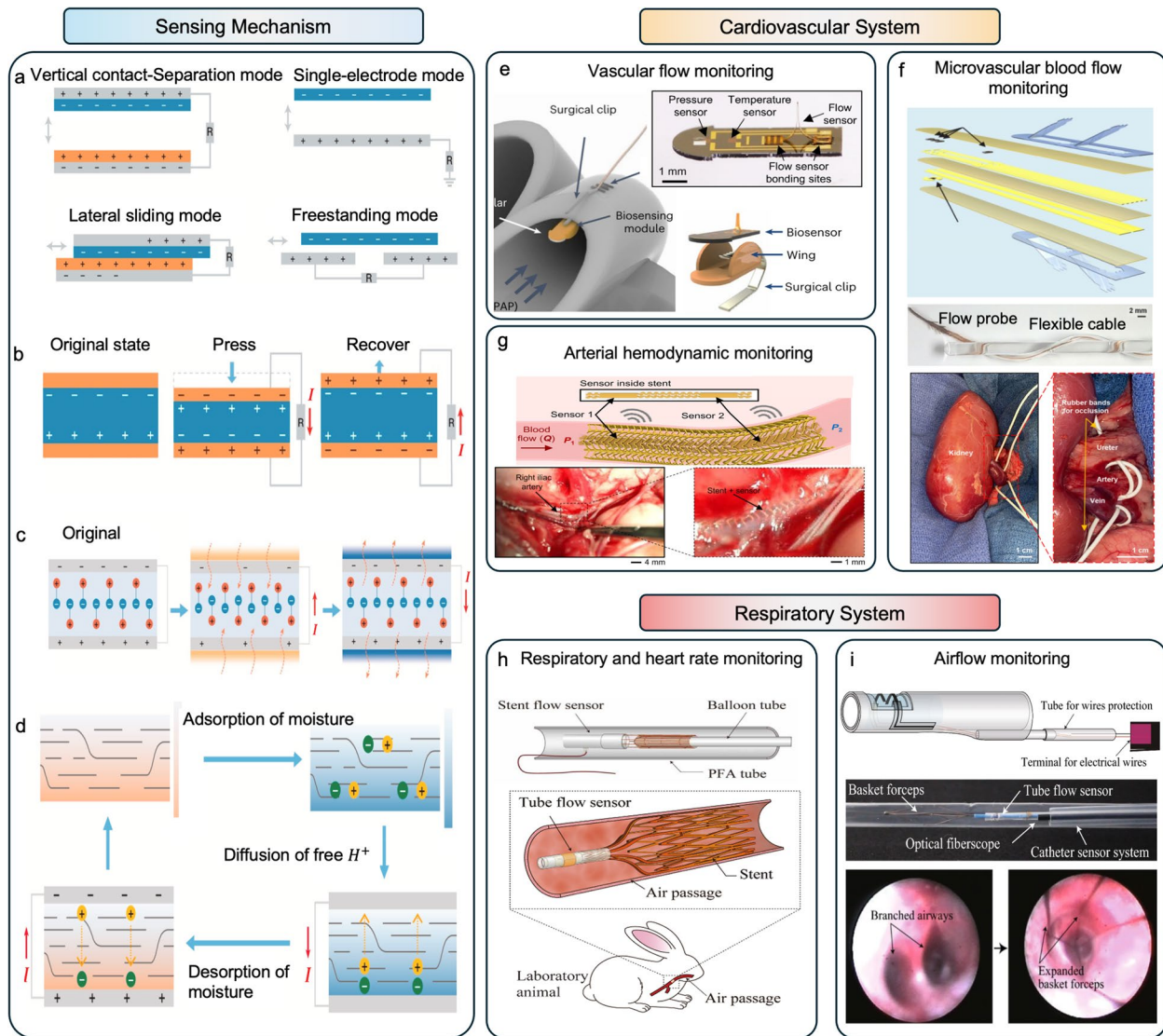


Fig. 4 Sensing mechanisms and applications of representative implantable flow sensors in monitoring blood flow in the cardiovascular system and airflow in the respiratory system. **a** Illustrations of four TENG sensing mechanism. Adapted and modified from [149]. **b** Schematic diagrams of PENG. Adapted and modified from [149]. **c** Schematic of the pyroelectric effect. Adapted and modified from [149]. **d** Schematic diagrams of the hydroelectric effect. Adapted and modified from [149]. **e** Schematic illustration of a flow sensor design, featuring a multi-sensing module implanted inside the pulmonary artery. Adapted and modified from [151]. **f** Schematic illustration and photograph of a flow probe with a porcine model kidney for blood flow control. Adapted and modified from [152]. **g** Schematic illustration and images of a wireless stent system implanted in a rabbit's artery. Adapted and modified from [20]. **h** Illustrations of a stent flow sensor and its applications for respiratory monitoring. Adapted and modified from [26]. **i** A catheter sensor system for in situ breathing measurements in the airway inside the lung. Adapted and modified from [153]

performance in both *ex vivo* and *in vivo* studies. The flow measurements are compared with those from commercial transonic flow transducers, demonstrating accurate detection of flow rate fluctuations. In *ex vivo* studies, the sensing module is inserted into pulmonary arteries (PAs). Flow measurements by the wireless system show a high correlation with commercial flow transducer data, with an average error of 0.5 ± 0.4 l/min for both forward and backward flows. In *in vivo* studies involve implanting the sensing module inside the

pulmonary artery. Continuous flow rate data reveal physiologically meaningful waveforms, with characteristic dips (dicrotic notches) observed during each pulse's downstroke. The wireless system is validated by comparisons with clinical standards, showing similar flow rate values and waveform characteristics. One limitation of this study is that the accuracy of blood flow measurements depends on proper sensor calibration. Variations in environmental conditions

Table 3 Summary of key parameters of representative implantable flow sensors

Implanted location	Mechanism	Main materials	Sensing performance	Ref
Pulmonary artery	Piezoresistive	Silicon, polyimide, gold, silicone	Gauge factor: 30 to 100 Average error: 0.5 ± 0.4 l/min	[151]
Kidney	Thermal	Gold, platinum, polyimide, cellulose acetate	Response time: 1–5 min Long-term stability: 9 days	[152]
Airway	Thermal	Polyimide, chromium, gold, copper	Airflow rates: 0–300 ccm Response time: 130 ms Accuracy: 0.57% error margin	[26]
Lung	Thermal	Chromium, gold, parylene	Response time: 60 ms	[153]

could affect sensor performance, necessitating regular recalibration to ensure accurate data interpretation.

Thrombosis refers to the abnormal formation of a blood clot (thrombus) inside a vessel, obstructing blood flow. In severe cases, it can block circulation, causing ischemia and tissue death [154]. Moreover, hepatic artery thrombosis is the second leading cause of liver graft failure, following primary graft nonfunction [155]. Hence, effective blood flow sensing allows for early intervention to help prevent graft failure [156]. In vivo thermal probes, such as those used for intracranial thermal microvascular flow sensing, can be used for continuous monitoring of cerebral perfusion [157]. Lu et al. have proposed an innovative wireless thermal-flow sensor, a miniaturized system utilizing a sub-millimeter scale and multi-nodal thermal probe to measure the microvascular blood flow [152]. This advanced flow probe incorporates multiple temperature sensing nodes, detecting temperature changes induced by blood flow. As blood flows through the tissue, convective heat transfer changes the temperature distribution around the sensor. The temperature distribution is used to estimate the blood flow velocity. The probe incorporates biodegradable cellulose acetate barbs to secure the probe to surrounding soft tissues, ensuring stability for up to nine days before degrading and facilitating easy removal. Insulated copper wires are sealed within a flexible silicon cable and connected to a BLE module encapsulated in Ecoflex in the assembly (Fig. 4f). The overall dimensions are comparable to a #12 biopsy needle (~2 mm diameter), allowing for minimally invasive insertion. The sensor's performance is evaluated using porcine models in vivo. The porcine kidney is selected to simulate artery thrombosis, with the sensor deployed by puncturing the kidney's capsule. In muscle flaps and kidneys of porcine models, the measured flow velocities (0.9–2.0 mm/s) and perfusion (4.1–8.2 mL/100 mL min for flaps, 35 mL/100 mL min for kidneys) are consistent with characteristics observed in previous reports. The sensor's response to simulated venous and arterial thrombosis is considered fast enough for 1–5 min. However, obtaining stable baseline temperature readings for accurate temperature change measurements is challenging.

The thermal conductivity of tissue may not be uniform, which can cause flow estimation errors.

Wireless implantable devices for continuous hemodynamic monitoring offer several significant benefits. More specifically, stents can facilitate robust wireless communication, ensuring reliable data transmission without the need for external wires. Herbert et al. have introduced a fully implantable, wireless, and batteryless vascular electronic system integrated with printed soft sensors [20]. The system utilizes a multimaterial inductive stent that serves as a backbone for wireless operation. The stent design includes conductive loops and non-conductive connectors, forming an inductive antenna (Fig. 4g). The sensors monitor hemodynamics in real-time, including arterial pressure, pulse rate, and flow. This is achieved through inductive coupling, allowing the stent to communicate wirelessly with an external loop antenna and VNA. The system measures changes in the resonant frequency to detect pressure variations and flow rates. A small inductive stent with an initial diameter of less than 1.5 mm and an expanded diameter of up to 3.0 mm is used for implantation. The inner surface of the stent is laminated with soft, low-profile capacitive sensors. The system's performance has been validated in artery models and through minimally invasive catheter implantation in an in vivo rabbit study. The system demonstrates a resolution of 5 mmHg in static air pressures and can detect sudden, large pressure changes. In vivo studies validate long-term stability, where the device maintained the functionality over several months. One limitation of this work is that the wireless measurements in vivo can be unreliable due to the small size of the artery and the distance between the implanted device and the skin. This can affect the quality and reliability of the transmitted data.

Respiratory system

An implantable flow sensor also plays a critical role in the respiratory system to measure airflow in the airways of animals to capture both respiration and heart rates [26]. Traditional methods, such as body plethysmography involving placing animals in a chamber to measure respiratory

functions based on pressure changes, have several limitations [26]. The method is sensitive to both body and environmental temperatures. As a result, animal movements can cause pressure variations, which makes it difficult to obtain accurate respiratory data. To address the limitation, Noma et al. have developed a stent flow sensor to measure respiratory and cardiac functions in unrestrained laboratory animals [26]. The sensing mechanism involves a combination of a heater and two temperature sensors integrated into a micro-machined tube, where the heater functions as a hot-wire anemometer. The flow rate is measured by the amount of electrical power needed to maintain a stable heater's temperature. The tube flow sensor and stent are assembled in a connection area and the stent expands mechanically to fit inside the airway (Fig. 4h). The sensor output increases with the flow rate, following the King's equation for hot-wire anemometry [158]. The stent flow sensor is implanted into the airway of anesthetized rats. The sensor is positioned at the center of the airway, where the flow velocity is the highest to maximize the sensitivity and accuracy of the flow measurements. The obtained respiration frequency is around 0.61 Hz, and the tidal volumes are measured at approximately 1.06 mL during expiration and 1.33 mL during inspiration, fitting within the physiological range for rats. The limitation of this sensor is that the stent structure relies on mechanical expansion to stay in place, which may introduce stress on the sensor and stent over time, especially in environments where movement is present or long-term stability is required.

Similarly, Maeda et al. have introduced the application of a catheter sensor system designed for in situ breathing and optical imaging measurements within the airways of the lung [153]. The system integrates a tube flow sensor with medical basket forceps and an optical fiberscope, all housed within a small-diameter tube for insertion into the airway. The system measures both airflows and captures optical images within the airways in real-time. The system utilizes a thermal air-flow sensor based on hot-wire anemometry. Two heaters are placed within the tube to measure airflow velocity and direction. Heat is carried away as air flows over the heaters, causing a measurable change in electrical power consumption. The sensor is attached to the inner tube of the catheter system with electrical connections made through enameled wires. The sensor's response is calibrated using King's law:

$$V^2 = A + Bu^n, \quad (7)$$

where V is the voltage supplied to maintain the heater, u is the flow velocity of the air, and A , B , and n are constants determined by the sensor design and structure. The optical fiberscope captures real-time images of the airway, assisting with positioning the catheter and monitoring the sensor's placement. The fiberscope guides the system to the desired location in the airway. The catheter sensor system is inserted

into the rabbit's airway, comprising the tube flow sensor and the optical fiberscope (Fig. 4i). Breathing airflow and optical images are successfully measured with a breathing cycle period of 1.08 s, which is consistent with the rabbit's physiological breathing rate. The catheter sensor system, with its thermal flow sensor and integrated optical fiberscope, provides a robust and precise method for in situ measurement of airflow and imaging within the airways.

Temperature sensors

Extensive research has indicated that organ temperature is closely related to organ vitality, inflammation, and infection [13, 159, 160]. Despite small temperature differences among various organs, temperature becomes a crucial warning signal under abnormal conditions. For instance, nerve damage or infection may result in an abnormal temperature increase of approximately 1°C within a few hours, whereas organ transplant rejection, such as kidney transplant rejection, can lead to a sharp temperature drop of several degrees Celsius within a single day [12, 19]. By continuously monitoring changes in organ temperature, implantable temperature sensors can provide critical support for disease prevention and treatment. These sensors enable long-term monitoring of organs, providing vital information for early warning and disease diagnosis. They are particularly useful for detecting organ diseases and wounds or postoperative infections, as abnormal temperature fluctuations are closely associated with various inflammations. In disease treatment, implantable temperature sensors can monitor the temperature around the treatment area, providing effective feedback for thermal effects in therapies and even forming closed-loop treatment systems. Monitoring and controlling tissue temperature is essential to prevent heat damage during therapies involving electrical or thermal stimulation. In some cases, these sensors can also deliver electrical or thermal stimulation, making them suitable for therapeutic interventions. Furthermore, temperature sensors can be part of multifunctional monitoring platforms when combined with other sensors, enabling signal calibration and enhancing the accuracy of medical assessments.

Compared to traditional temperature measurement devices, implantable temperature sensors must be small, thin, flexible, and nontoxic to achieve mechanical and biological compatibility with organs, allowing long-term monitoring with minimal tissue damage. These specific requirements make it impossible to adapt commonly used "gold standard" mercury thermometers into implantable formats. Additionally, many optical-based temperature sensors, such as infrared thermometer, are unsuitable for organ temperature monitoring due to the water content of organs and the barrier properties of the skin. Currently, the most commonly

used implantable temperature sensors can be categorized based on their mechanisms: resistance temperature detectors (RTDs), thermocouple temperature detectors, dielectric constant temperature detectors, Positive-Intrinsic-Negative (PIN) diode temperature detectors, temperature sensing oscillators, and meta-structured temperature detectors. The most common sensing mechanism is based on the change in electrical resistance with temperature, as seen in RTDs. RTD temperature sensors, typically made from metals such as platinum (Pt), copper (Cu), and nickel (Ni), can achieve measurement accuracy ranging from 0.1 to 0.5°C with a potential maximum accuracy of 0.05°C or even higher [161]. The predictable linear relationship between a wire's electrical resistance and temperature enables precise temperature measurements. For measuring temperatures within the human physiological range (~30–45°C), the relationship between resistance and temperature can be expressed as [161]: $R_T = R_0(1 + \alpha T)$, where α is the temperature coefficient, T is the temperature, R_T is the resistance at temperature T , and R_0 is the resistance at the reference temperature. The advantages of RTDs include stable and repeatable resistance–temperature relationship, as well as flexibility in the sensor design. By arranging the wire in various configurations, these sensors can be customized to meet specific organ temperature sensing requirements. For implantable temperature sensors, the common design of RTD to minimize local strain is the use of thin and narrow microwires embedded in a sandwich structure using lithographic techniques, resulting in an ultrathin and compact sensing area (Fig. 5a). Examples include the gold thermal sensing disk with a thickness of 100 nm and a line width of ~20 μm , and the 200-nm-thick serpentine-shaped MoS_2 temperature sensor [12, 162]. The small and thin features enable them to conform seamlessly to the organ. Moreover, the fabrication of RTDs is compatible with existing planar manufacturing processes, which allows convenient construction of multifunctional monitoring platforms. Thermocouple temperature sensors operate based on the thermoelectric effect (Fig. 5b). Specifically, in a closed loop formed by two different metals, A and B, an electromotive force is generated in the presence of a temperature difference between the two metals, resulting in a measurable current flow [163]. The relationship between the temperature (T) and the output voltage (V_s) of a thermocouple can be expressed as [161]: $V_s(T) = \sum_{i=0}^n a_i \cdot T^i$, where a_i represents the i^{th} coefficient of the polynomial, and n denotes the order of the polynomial. The values of a_i and n vary depending on the type of thermocouple and the specific temperature range. Thermocouples are known for their stability, fast response, and small heat capacity, making them suitable for the calibration of other types of temperature sensors [164]. The dielectric constant temperature detection is another commonly used method. The dielectric constant (ϵ_r) is a property of sensing materials that quantifies the ability

of an insulator to store electrical energy within an electric field [165]. By exploiting the temperature dependence of the dielectric constant, temperature sensors can be developed to influence the performance of LC circuits. For example, polyethylene glycol (PEG) is known for its pronounced temperature-dependent dielectric constant, particularly within the 34–42 °C range, which corresponds to typical human body temperatures. This temperature dependence can be analytically described by the Curie–Weiss formula:

$$\epsilon_r = \epsilon_s + (\epsilon_l - \epsilon_s) \frac{T_m - T_C}{T - T_C} (T < T_m), \quad (8)$$

where ϵ_s and ϵ_l are the dielectric constants of the solid phase at low temperature and the liquid phase at the melting temperature, while T_m and T_C are the melting temperature and effective Curie temperature determined by the molecular weight M_w of PEG, respectively. An LC circuit can be constructed by using PEG to fabricate a capacitor and by connecting the capacitor to an inductor (with inductance L and resistance R), which will resonate at a certain frequency. Therefore, temperature sensing can be realized by coupling this circuit with a secondary coil linked to a specialized signal readout system [165]:

$$f_s = 1/2\pi\sqrt{LC} = f_s(T) \quad (9)$$

In addition to common conductors, PIN diodes also exhibit obvious temperature dependence. Specifically, its turn-on voltage varies with temperature [166]. This implies a linear relationship between voltage and temperature at a fixed current, or between diode current and temperature at a fixed voltage. Building on this mechanism, Sahasrabudhe et al. have developed a temperature sensor using diodes ($\text{In}_x\text{Ga}_{1-x}\text{N}$) to monitor heat dissipation in tissues during surgical procedures [164]. Moreover, since the diode is a small electronic component with a unique temperature-dependent I-V relationship, a diode connected to an LC circuit can be used to construct a temperature sensing oscillator. For example, Chen et al. have combined stacked NMOS diodes into an LC circuit, forming a temperature-dependent oscillator [170]. The oscillation frequency of the oscillator can be designed to vary with temperature by exploiting the temperature dependence of the leakage current flowing through a subthreshold-biased transistor, thereby achieving temperature sensing through frequency feedback. In addition to electrical signal-based sensing mechanisms, an alternative approach involves using materials with inherent temperature-dependent properties, such as temperature-sensitive acoustic materials (Fig. 5c). For example, Tang et al. have developed a series of temperature sensors based on meta-structured hydrogels (metagels) [46]. These metagels can sense the intracranial temperature by responding to temperature-induced micro-deformations. The metagel comprises a

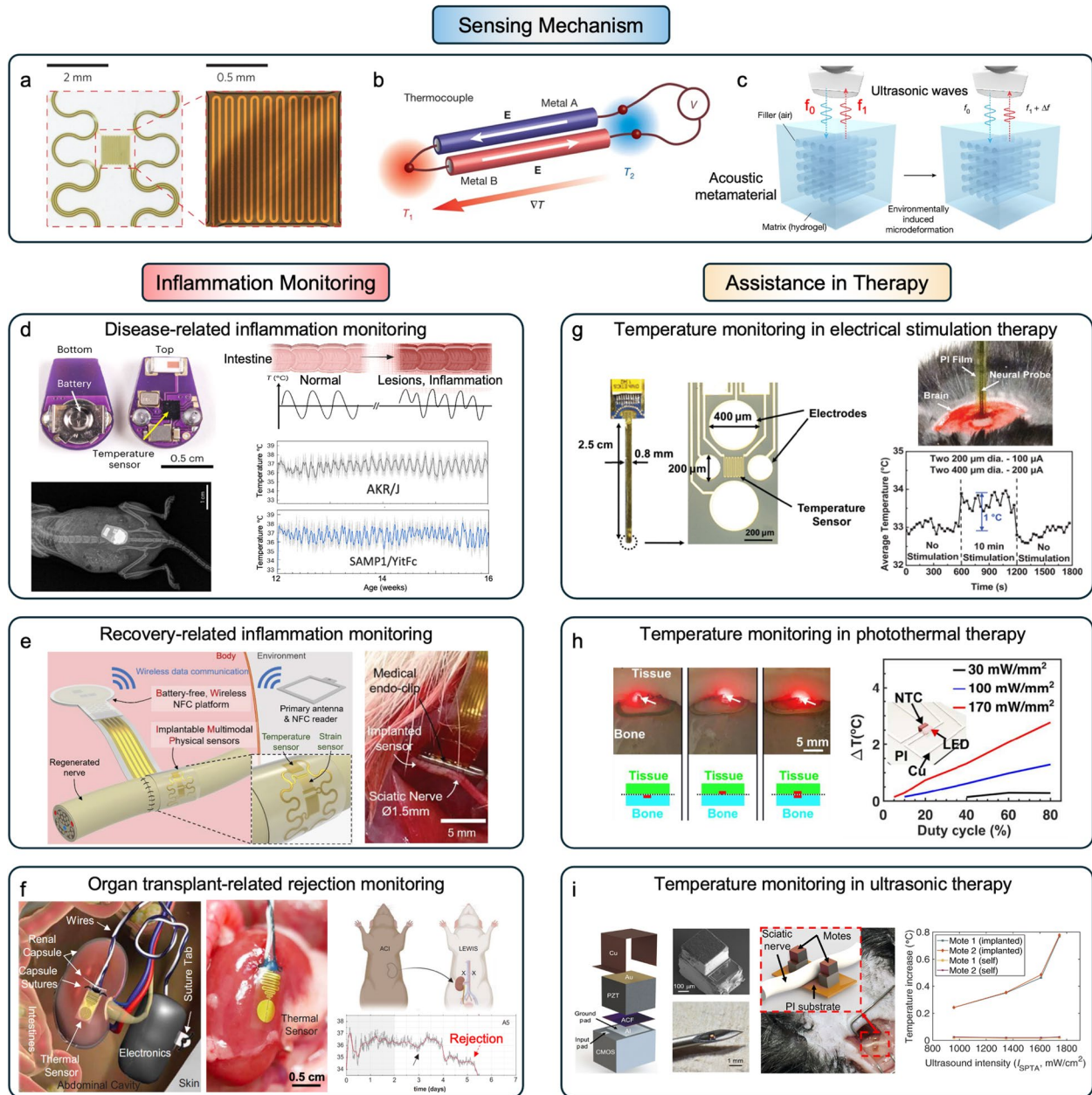


Fig. 5 Implantable temperature sensors and their applications in monitoring inflammation and assisting therapy. **a, b, c** Representative sensing mechanisms for implantable temperature sensors: (a) resistance temperature detectors, adapted and modified from [166]; (b) thermocouples, adapted and modified from [167]; (c) meta-structured temperature detectors, adapted and modified from [46]. **d** A wireless implantable temperature sensor for long-term monitoring of characteristic temperature patterns in intestinal Crohn's disease. Adapted and modified from [22]. **e** A cuff-type implantable temperature sensor for monitoring inflammation in recovering sciatic nerve injuries. Adapted and modified from [19]. **f** An implantable temperature sensor patch for monitoring kidney transplant rejection. Adapted and modified from [12]. **g** A neural probe integrated with a temperature sensor for real-time monitoring during electrical brain stimulation. Adapted and modified from [168]. **h** A photothermal therapy patch with an integrated temperature sensor for real-time monitoring during bone treatment. Adapted and modified from [27]. **i** An acoustic temperature sensor for synchronous temperature feedback during focused ultrasound therapy. Adapted and modified from [169]

hydrogel matrix embedded with periodic air columns, forming a soft phononic crystal with tunable acoustic reflection spectra. As the temperature changes, the hydrogel undergoes micro-deformations, altering its acoustic properties and leading to shifts in the acoustic reflection spectra. In this

system, the metagel exhibits a strong correlation between frequency and temperature across a wide range of 28–43 °C, encompassing the typical range of human core body temperature. This method avoids direct electrical signals and

transmission, offering potential for long-term implantation of temperature sensors [46].

Inflammation monitoring

The development of various types of implantable temperature sensors has revolutionized several critical areas in modern healthcare, including organ disease monitoring, wound/postoperative recovery tracking, and assistance in precision therapy. Inflammation is a biological response of the immune system, triggered by various factors such as pathogens, damaged cells, and toxic compounds. Inflammation can be associated with various scenarios, including tissue and organ infections, inflammatory diseases, and organ transplant rejection. Implantable temperature sensors have the potential to revolutionize the monitoring and timely treatment of inflammation. For example, Crohn's disease, a chronic inflammatory bowel disease, can affect any part of the gastrointestinal tract and penetrate deep into the bowel tissue. As a lifelong condition with periods of remission and flare-ups, Crohn's disease requires long-term monitoring [21]. Existing monitoring techniques, including surveillance endoscopy, MRI, computed tomography (CT), and ultrasound imaging are not only cumbersome and complex, but also incapable of providing real-time monitoring capabilities [171]. The intestinal temperature variations associated with Crohn's disease make long-term monitoring strategies based on temperature sensors feasible. Madhvapathy et al. have developed a small ($12.8 \times 8.2 \times 5.8 \text{ mm}^3$), lightweight ($\sim 0.58 \text{ g}$), smooth (roughness $S_a = 2.8 \pm 1.6 \text{ }\mu\text{m}$), and biocompatible intestinal temperature sensor for monitoring and treating intestinal inflammation (Fig. 5d) [22]. The shape and surface design avoid adhesion, tissue necrosis, and imbalance of intestinal microbial flora caused by friction between the sensor and the intestinal lining [172, 173]. The button battery-powered system and low-power Bluetooth chip enable the temperature sensor to report intestinal temperature continuously for 16 weeks for long-term and real-time monitoring of inflammatory events during the progression of Crohn's disease without adverse effects. Compared to complex traditional medical equipment, this simple sensor offers new possibilities for long-term disease monitoring. In addition to disease-related inflammation, implantable temperature sensors are valuable in monitoring inflammation associated with wounds or postoperative recovery. For example, monitoring nerve healing is crucial as incomplete or suboptimal recovery can lead to permanent physical disabilities near the repaired nerve. Traditional monitoring methods are often complex, requiring highly trained technicians, and may pose a risk of secondary nerve damage during the assessment [174]. Infection and inflammation during wound recovery often cause localized temperature changes due to increased vascular

permeability, making temperature sensor-based monitoring a viable approach for assessing recovery [175]. Kim et al. have designed a $35 \text{ mm} \times 4 \text{ mm} \times 100 \text{ }\mu\text{m}$ ($L \times W \times T$) cuff-type flexible sensor, consisting of Au microcircuits embedded within a PI film and encapsulated in the biocompatible Ecoflex layer (Fig. 5e) [19]. The thin, cuff-type design of the sensor reduces the impact of the polymer encapsulation layer on thermal conductivity and allows it to be wrapped closely around the injured sciatic nerve and fixed with an endo-clip, enabling real-time monitoring of temperature changes. The elastic modulus of Ecoflex ($< 70 \text{ kPa}$) is lower than those of typical peripheral nerves of mammals, which reduces the risk of damaging sensitive nerves during sensor implantation. As a result, this temperature sensor can monitor nerve changes throughout the recovery process, offering early detection of serious nerve damage or unexpected complications based on abnormal temperature fluctuations during recovery. Moreover, organ rejection can also lead to significant inflammation. For instance, 10% to 15% of kidney transplant recipients experience subclinical rejection within the first few months to a year, leading to inflammation and potential organ failure. If rejection is detected early, timely treatment can preserve organ function. The current "gold standard" for detecting rejection reactions, namely biopsy, has several limitations in providing timely warnings of rejection. They carry the risk of false positives and negatives, and can cause pain, bleeding, infection, and other complications for patients [176–178]. Temperature changes associated with organ rejection have the potential to revolutionize rejection monitoring. Madhvapathy et al. have developed a small ($\sim 0.3 \times 0.7 \text{ cm}^2$), ultrathin ($\sim 220 \text{ }\mu\text{m}$), stretchable (20% stretchability), flexible (bending radius $\geq \sim 2.8 \text{ mm}$), smooth ($0.13 \text{ mm} \pm 0.02$ areal surface roughness) and biocompatible (encapsulated by layers of polyimide and silicone) temperature sensor that can be attached to the kidney via a direct surgical suture, thereby enabling real-time monitoring of kidney transplant-related rejection reactions (Fig. 5f) [12]. The internal battery can maintain the system's surface temperature and support thermal conductivity monitoring for about 30 days, or up to 8 months if used solely for temperature monitoring, which covers the period of highest risk for organ rejection. Abnormal temperature signals, such as sudden drops, can serve as important indicators of organ rejection. This real-time diagnostic method is convenient for both doctors and patients. Implantable temperature sensors have opened new possibilities for timely and convenient detection of inflammation. One common limitation of temperature sensors is their dependence on battery life and Bluetooth transmission. To overcome this, passive sensing and special transmission strategies have been proposed to reduce power consumption or even eliminate the need for power. For instance, Karipott et al. have integrated a resonant circuit sensor with an existing orthopedic implant to

detect post-surgical inflammation. This allows for remote monitoring of the temperature near the implant through inductive coupling with an external detection coil [179]. Similarly, Kim et al. have used NFC to form a battery-free and wireless monitoring sensor platform, enabling external devices to read the sensor signals [19]. Despite the advantages of this method, heating during electromagnetic wave transmission remains a potential concern. In contrast, Maini et al. have designed a passive temperature sensor using acoustic metamaterials. The sensor consists of a PDMS matrix embedded with micropillars that reflect ultrasonic waves. It detects temperature variations by altering the frequency of the reflected waves as the matrix deforms due to thermal expansion. This strategy eliminates the need for internal power and data transmission, making it particularly advantageous for long-term implantation and sustained biocompatibility [180].

Assistance in therapy

Beyond inflammation monitoring, implantable temperature sensors also play a crucial role in assisting therapy. Treatment methods for organ, nerve, and tissue diseases, including electrotherapy, thermal therapy, phototherapy, and focused ultrasound therapy (FUS), often lead to localized heat accumulation. During treatment, it is typically essential to regulate the temperature and its impact range to prevent undesirable damage to healthy cells. In these scenarios, implantable temperature sensors can provide precise temperature feedback and facilitate the formation of a closed-loop therapy system. For example, neural probes, which deliver electrical stimulation through their electrodes, play a crucial role in treating neurological and brain diseases such as Alzheimer's, Parkinson's, and epilepsy [181, 182]. Simultaneously, the negative effects of electrical stimulation, such as instantaneous temperature increases and localized heat accumulation, should be minimized to prevent unintentional damage to delicate brain cells. To address this issue, Wang et al. have integrated temperature sensors into neural probes for real-time monitoring of local temperature during electrical stimulation (Fig. 5g) [168]. The neural probe features two sets of electrodes, with a temperature sensor composed of a 5 μm linewidth Au serpentine microcircuit (RTD type) positioned at the center of the electrodes. The entire probe is encapsulated in a 1 μm thick layer of PI, which ensures biocompatibility while minimizing the impact of polymer thickness on the thermal conductance. As a result, the probe can accurately record local temperature changes of several degrees Celsius during electrical stimulation of the brain and eyes. This integration eliminates the need for additional surgery to implant traditional, larger thermometers in the target area. Implantable temperature sensors used in photothermal therapy can provide similar feedback. Light and

heat therapies are valuable for bone healthcare, including in the treatment of osteoporosis and the recovery from fragility fractures. Based on this, Cai et al. have developed a bone healthcare patch that combines a microscale inorganic light-emitting diode (μ -ILED) with a temperature sensor, enabling both bone treatment and real-time monitoring of local temperature changes (Fig. 5h) [27]. The entire device has been through three encapsulation treatments: first with silane, followed by two layers of 9 μm parylene-C, and finally a PDMS dip coating. To further ensure long-term implantation and stability, the device is anchored on the bone by utilizing calcium phosphate ceramic particles in combination with transforming growth factor beta 1 (TGF- β 1) [183]. This integrated device can operate continuously for weeks without adverse effects. However, this nearly permanent implantation method raises important considerations regarding device removal post-treatment and the potential risks in human applications. In addition to integrating sensors with therapeutic devices, another approach is to design small-sized passive implantable temperature sensors to provide temperature feedback during long-term treatment. For example, Shi et al. have designed ultra-small implantable temperature-sensing oscillators made of lead zirconate titanate, with a volume of only 0.065 mm^3 (Fig. 5i) [169]. This sensor is compact enough to be delivered through an 18-gauge microneedle and injected directly into the target tissue, minimizing inconvenience during or after implantation. The temperature-modulated signal from the sensor can be transmitted back to the ultrasound source via acoustic backscattering, which is particularly valuable for assessing the thermal effects of medical procedures such as focused ultrasound neuromodulation. When coated with an 8- μm -thick layer of parylene C, the sensor exhibits no functional or performance degradation during continuous soaking in PBS for over 21 days, making it highly suitable for long-term implantation. Similarly, this passive acoustic feedback consists of polymer acoustic microstructures and contributes to prolonged implant stability, as it does not contain any metal components [180]. Clearly, implantable temperature sensors have demonstrated significant value in providing assistance in therapy. Small, thin implantable temperature sensors offer significant benefits for both patients and doctors by enabling real-time temperature monitoring, supporting precision medicine, and preventing accidental damage from overheating.

Representative examples of implantable temperature sensors are summarized in Table 4.

Conclusions and outlook

Implantable physical sensors have the potential to revolutionize medical and healthcare practices by enabling direct, real-time acquisition of critical physiological signals from

Table 4 Summary of key parameters of representative implantable temperature sensors

Function and implanted location	Mechanism	Main materials	Sensing performance	Ref
Inflammation monitoring (kidney)	RTD	Gold, polyimide, silicone	Range: 30–41°C Resolution: ~0.004°C Accuracy: ±0.1°C Response time: ~0.13 s Long-term stability: > 27 days	[12]
Inflammation monitoring (nerves)	RTD	Gold, polyimide, ecoflex	Range: 0–40°C Signal-to-noise ratio: 100 Sensitivity: 0.22%/°C Response speed: 8°C/s Long-term stability: > 21 days	[19]
Inflammation monitoring (bones)	Acoustic	Silicon, PDMS	Range: 29–43°C Resolution: ~0.03 K	[180]
Inflammation monitoring (brain)	Acoustic	Polyvinyl alcohol/ poly(N-isopropylacrylamide) (PVA/PNIPAM)	Range: 28–43°C Resolution: 0.1°C Sensitivity: 80 kHz/°C Long-term stability: 3–4 weeks	[46]
Assistance in therapy (brain and retina)	RTD	Gold, chromium, polyimide	Range: 18–42°C Accuracy: ±0.25°C Response time: 1.3 s	[168]
Assistance in therapy (bones)	Thermistor	Polyimide, copper, NTC thermistor, Parylene, PDMS, calcium phosphate ceramic particles	Range: 33–41°C Resolution: 10 mK Sensitivity: ~1920 ADC/K Long-term stability: 205 days (estimated)	[27]
Assistance in therapy (nerves)	Relaxation oscillator	Lead zirconate titanate, gold, copper, aluminum, anisotropic conductive film, CMOS, parylene	Range: 25–50°C Resolution: ~0.049°C Accuracy: ±0.2°C Response time: ~0.13 s Long-term stability: > 21 days	[169]

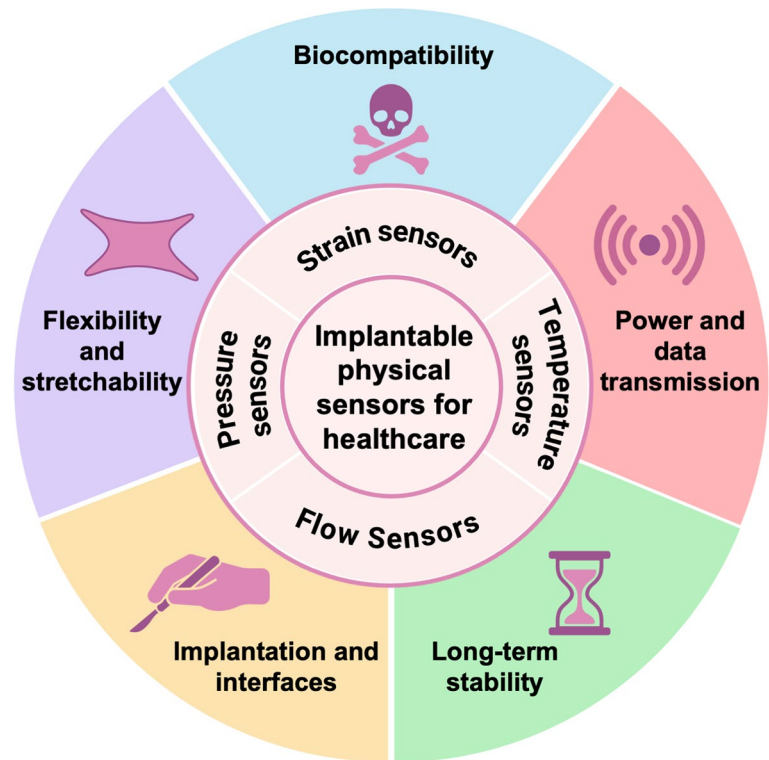
internal organs and tissues. These sensors—including strain, pressure, flow, and temperature sensors—may significantly advance patient care, facilitate early diagnosis, and enhance treatment efficacy across various medical disciplines. Implantable strain sensors are vital for monitoring biomechanical changes within organs, muscles, and bones, providing crucial data on organ volume fluctuations, tissue stiffness, and motion rhythms. This information is essential for assessing post-surgical recovery and managing chronic conditions. Implantable pressure sensors, particularly those used to monitor ICP and cardiovascular parameters, deliver real-time data critical for managing traumatic brain injuries, heart diseases, and hypertension. Similarly, implantable flow sensors, especially in vascular applications, enable continuous monitoring of blood flow, which is essential for managing conditions such as aneurysms and atherosclerosis. Implantable temperature sensors play a dual role: they monitor organ health, inflammation, and infection, while also integrating with therapeutic tools to regulate tissue temperature during treatments such as electrotherapy and photothermal therapy, thereby supporting precision medicine and enhancing treatment safety. Unlike wearable sensors, implantable sensors must address a range of complex

factors, including biocompatibility, flexibility, and stretchability, implantation procedures, long-term stability, as well as power and data transmission (Fig. 6). These considerations are critical to ensuring the successful integration and reliable performance of implantable sensors within the human body over extended periods.

Material biocompatibility

The biocompatibility of materials used in implantable sensors is crucial, as it directly influences organ health and can potentially trigger immune responses. In the design process, priority should be given to FDA-approved metallic materials such as titanium, platinum, 316 L stainless steel, magnesium, nitinol, gold, and silver for use in electronic components [184]. Similarly, FDA-approved polymers such as PEG, polyethylene terephthalate (PET), parylene, polytetrafluoroethylene (PTFE), and polyurethane (PU) should be preferred for use as substrate or encapsulation materials [184, 185]. Additionally, materials such as TiO₂, SiO₂, Al₂O₃, PLGA, and PDMS have been validated as non-cytotoxic in a large number of studies [120, 186–189]. Magnesium, zinc, PLGA have also been well-documented

Fig. 6 Key considerations in the design, testing, and in vivo performance of implantable physical sensors



as bioabsorbable, degradable, or excretable materials [122]. However, the potential toxicity of emerging nanomaterials such as metal nanowires and CNTs remains unclear [190, 191]. Although initial cytotoxicity tests have indicated low toxicity levels, more rigorous and long-term studies are essential to confirm their biocompatibility, particularly in human cells and across diverse cell models.

Long-term stability

The long-term stability of implantable sensors is essential for ensuring accurate measurements and safeguarding organ health. Sensors that lose stability over time can produce erroneous data, compromising patient safety. Effective encapsulation is key to maintaining this stability. Materials such as parylene, known for their low water vapor transmission and oxygen permeability, can protect sensitive components from corrosion or oxidation [192]. Tables 1, 2, 3 and 4 indicate that sensors utilizing effective encapsulation materials, such as parylene, typically exhibit long-term stability. Additionally, the long-term performance of sensors can be compromised by chemical and mechanical aging, including cyclic stresses, compressions, and prolonged exposure to body fluids, which may lead to material degradation and affect sensors' mechanical and electrical properties [98, 193]. It is also crucial to understand yield and fatigue limits of materials. Furthermore, battery life plays a significant role in sensor longevity. The need for battery replacement or

recharging in implantable devices is inconvenient and risky, making the development of low-power systems or battery-free designs critical strategies for enhancing long-term stability [164]. In contrast to sensors requiring long-term stability, bioresorbable sensors offer a conceptually different approach by operating only for a predetermined period before safely dissolving within the body [162, 189]. This eliminates the need for sensor removal and reduces potential risks associated with secondary surgery. Challenges for bioresorbable sensors mainly lie in achieving stable sensor performance and control over the dissolution process, which may require advanced structural design, material selection, and novel encapsulation strategies to ensure reliable performance during the sensor's intended operational period.

Mechanical flexibility and stretchability

When selecting materials for implantable sensors, flexibility and stretchability must be carefully considered to minimize mechanical mismatch between the devices and the target organ or tissue. For example, sensors designed for the bladder need to exhibit significant stretchability, often exceeding 70%, while materials for brain implants require a low elastic modulus (0.5–3 kPa) to match the softness of brain tissue (Fig. 1). Mechanical mismatch can adversely affect both signal quality and organ health. To address these challenges, intrinsically stretchable conductors can be used, such as silver nanoparticles, silver nanowire networks and

liquid metals, while stretchable elastomers such as PDMS and Ecoflex can serve as substrates or encapsulation layers [194–197]. Additionally, structural designs such as serpentine layouts [198] and kirigami designs [199, 200] can be leveraged to create structurally stretchable components using materials with limited strain limit, such as metals (e.g., gold, titanium) and dielectric materials (e.g., SiO₂, parylene) [201, 202]. These designs enable the integration of materials that are not inherently stretchable, ensuring that the sensors can conform to and move with the body's tissues without compromising functionality.

Implantation and device-tissue interfaces

The choice of implantation method for implantable sensors influences their functionality and their impact on organ health. An optimal method should minimize tissue damage, reduce infection risk, and ensure precise sensor placement and intimate sensor-tissue interface for reliable measurements. Traditional surgical suturing is commonly used to anchor sensors on or within tissues [12, 98]. Although suturing offers stable sensor attachment, it can lead to tissue damage, inflammation, and complications such as scarring and bleeding during both implantation and retrieval. Bioadhesives composed of soft polymers or hydrogels present a less invasive alternative by adhering to wet tissue surfaces through physical or covalent cross-linking mechanisms, such as hydrogen and amide bonds [164, 203, 204]. These adhesives can minimize tissue trauma and reduce bleeding; however, their adhesion strength can vary based on the tissue type and physiological conditions, and their long-term stability under dynamic conditions remains a potential challenge. Novel bio-inspired adhesives with strong yet reversible adhesion to organ and tissue surfaces may lead to more reliable sensor-tissue interfaces [205, 206]. In addition, the use of smart materials that respond to physiological changes could enable dynamic adaptation of the sensor-tissue interface, enhancing sensor stability and function over time. Innovations in minimally invasive delivery methods, potentially through the use of advanced robotics and imaging technologies, could improve sensor placement accuracy and reduce tissue damage.

Power supply and data transmission

Power and signal transmission are essential for ensuring that implantable sensors operate effectively and transmit accurate data to external monitoring systems. Typically, these sensors are powered by batteries, such as coin-cell batteries, which can be supplemented with wireless charging features such as RF coils [12, 207]. In addition, self-powered systems, including piezoelectric nanogenerators (PENGs) and TENGs, are emerging as promising alternatives by harvesting energy

from the body's own movements [208–210]. Traditional signal transmission methods, such as percutaneous wires, are generally discouraged due to the increased risk of infection and patient discomfort [211]. Instead, wireless transmission methods are preferred, with active systems such as Bluetooth offering a more convenient and patient-friendly solution. Passive wireless transmission designs, such as LC resonant circuits or chip-less radiofrequency identification (RFID), can eliminate the need for batteries, further extending sensor lifespan [212–214]. Additionally, novel passive transmission methods, such as metastructured hydrogels made entirely of polymers, are capable of converting micro-deformations into temperature feedback via acoustic backscattering [46, 170]. This approach is particularly advantageous for long-term implantation and sustained biocompatibility.

Bench-to-clinic translation

Translating implantable physical sensors from benchtop testing to human use is a complex process with several significant challenges. Standardized testing methods are recommended during benchtop testing for initial evaluation. For example, key tensile properties, such as elastic modulus, tensile strength, and elongation at break, can be evaluated using ASTM D412 for sensors made of elastomers and ASTM D882 for sensors made of thin plastic sheets. ASTM D4482 provides guidelines for investigating the fatigue life, hysteresis, and cyclic deformation of rubber materials [215]. For more a thorough device examination, ISO 14708–1 has specific testing standards to evaluate implantable devices under mechanical impact, vibration, temperature changes, and exposure to humidity [216]. Animal studies follow benchtop testing and are critical for assessing the feasibility, safety, biocompatibility, and long-term performance. However, differences between animal models and human biology can lead to unexpected outcomes in clinical trials [217]. Therefore, biocompatibility test standards such as ISO 10993 require a series of toxicity tests to allow medical devices to be used in clinic settings. Ensuring long-term biocompatibility and stability is another challenge, as sensors must function accurately over extended periods without triggering immune responses or degrading in the body. As many physical sensors are integrated into larger implantable devices, such as neurostimulators and bladder control systems, their integration with existing medical technologies in real-world clinical settings adds complexity that must be addressed during development. Another critical aspect of the translation process is the regulatory and compliance considerations. Stringent standards for safety, efficacy, device manufacturing quality, and other factors need to be met before implantable devices are approved for human use. To facilitate the bench-to-clinic translation, advances in material science, such as the development of new materials that

are more biocompatible with the human immune system, will be critical in improving sensor longevity and minimizing immune reactions. Additionally, innovations in simulation and modeling techniques may allow better prediction of the behavior of these sensors in the human body, potentially reducing reliance on animal models and accelerating the transition to human trials.

Acknowledgements H.Z. acknowledges the invitation of this review paper from the *Med-X* editorial board.

Authors' contributions X.L. and H.Z. initialized the project. X.L., X.H., L.Y., and S.J. prepared the figures. All authors wrote the original manuscript, revised the manuscript, and approved the final version.

Funding The authors acknowledge funding by the National Institutes of Health Center for Autonomic Nerve Recording and Stimulation Systems under award number 1U41NS129514.

Data availability The data that support the findings of this study are available from the corresponding author upon reasonable request.

Declarations

Competing interests The authors declare no competing interests.

Open Access This article is licensed under a Creative Commons Attribution 4.0 International License, which permits use, sharing, adaptation, distribution and reproduction in any medium or format, as long as you give appropriate credit to the original author(s) and the source, provide a link to the Creative Commons licence, and indicate if changes were made. The images or other third party material in this article are included in the article's Creative Commons licence, unless indicated otherwise in a credit line to the material. If material is not included in the article's Creative Commons licence and your intended use is not permitted by statutory regulation or exceeds the permitted use, you will need to obtain permission directly from the copyright holder. To view a copy of this licence, visit <http://creativecommons.org/licenses/by/4.0/>.

References

- Zhao C, Park J, Root SE, Bao Z. Skin-inspired soft bioelectronic materials, devices and systems. *Nat Rev Bioeng*. 2024;2:671–90. <https://doi.org/10.1038/s44222-024-00194-1>.
- Ray TR, Choi J, Bhandodkar AJ, et al. Bio-integrated wearable systems: a comprehensive review. *Chem Rev*. 2019;119:5461–533. <https://doi.org/10.1021/acs.chemrev.8b00573>.
- Kim J, Campbell AS, de Ávila BEF, Wang J. Wearable biosensors for healthcare monitoring. *Nat Biotechnol*. 2019;37:389–406. <https://doi.org/10.1038/s41587-019-0045-y>.
- Chen G, Xiao X, Zhao X, et al. Electronic textiles for wearable point-of-care systems. *Chem Rev*. 2022;122:3259–91. <https://doi.org/10.1021/acs.chemrev.1c00502>.
- Yang JC, Mun J, Kwon SY, et al. Electronic skin: recent progress and future prospects for skin-attachable devices for health monitoring, robotics, and prosthetics. *Adv Mater*. 2019;31:1904765. <https://doi.org/10.1002/adma.201904765>.
- Zhou Z, Chen K, Li X, et al. Sign-to-speech translation using machine-learning-assisted stretchable sensor arrays. *Nat Electron*. 2020;3:571–8. <https://doi.org/10.1038/s41928-020-0428-6>.
- Zhou Y, Zhao X, Xu J, et al. Giant magnetoelastic effect in soft systems for bioelectronics. *Nat Mater*. 2021;20:1670–6. <https://doi.org/10.1038/s41563-021-01093-1>.
- Yin J, Wang S, Tat T, Chen J. Motion artefact management for soft bioelectronics. *Nat Rev Bioeng*. 2024;2:541–58. <https://doi.org/10.1038/s44222-024-00175-4>.
- Zhao X, Zhou Y, Xu J, et al. Soft fibers with magnetoelasticity for wearable electronics. *Nat Commun*. 2021;12:6755. <https://doi.org/10.1038/s41467-021-27066-1>.
- Zhao X, Zhou Y, Song Y, et al. Permanent fluidic magnets for liquid bioelectronics. *Nat Mater*. 2024;23:703–10. <https://doi.org/10.1038/s41563-024-01802-6>.
- Hoare D, Kingsmore D, Holsgrove M, et al. Realtime monitoring of thrombus formation in vivo using a self-reporting vascular access graft. *Commun Med*. 2024;4:15. <https://doi.org/10.1038/s43856-024-00436-8>.
- Madhvapathy SR, Wang J-J, Wang H, et al. Implantable bioelectronic systems for early detection of kidney transplant rejection. *Science*. 2023;381:1105–12. <https://doi.org/10.1126/science.adh7726>.
- Fierheller M, Sibbald RG. A clinical investigation into the relationship between increased periwound skin temperature and local wound infection in patients with chronic leg ulcers. *Adv Skin Wound Care*. 2010;23:369–79. <https://doi.org/10.1097/01.ASW.0000383197.28192.98>.
- Budday S, Sommer G, Birk C, et al. Mechanical characterization of human brain tissue. *Acta Biomater*. 2017;48:319–40. <https://doi.org/10.1016/j.actbio.2016.10.036>.
- MacManus DB, Ghajari M. Material properties of human brain tissue suitable for modelling traumatic brain injury. *Brain Multiphys*. 2022;3: 100059. <https://doi.org/10.1016/j.brain.2022.100059>.
- Singh G, Chanda A. Mechanical properties of whole-body soft human tissues: a review. *Biomed Mater*. 2021;16: 062004. <https://doi.org/10.1088/1748-605X/ac2b7a>.
- Roccabianca S, Bush TR. Understanding the mechanics of the bladder through experiments and theoretical models: Where we started and where we are heading. *Technology*. 2016;4:30–41. <https://doi.org/10.1142/S2339547816400082>.
- Idzenga T, Farag F, Heesakkers J, et al. Noninvasive 2-dimensional monitoring of strain in the detrusor muscle in patients with lower urinary tract symptoms using ultrasound strain imaging. *J Urol*. 2013;189:1402. <https://doi.org/10.1016/j.juro.2012.09.165>.
- Kim S, Oh YS, Lee K, et al. Battery-free, wireless, cuff-type, multimodal physical sensor for continuous temperature and strain monitoring of nerve. *Small*. 2023;19:2206839. <https://doi.org/10.1002/sml.202206839>.
- Herbert R, Lim H-R, Rigo B, Yeo W-H. Fully implantable wireless batteryless vascular electronics with printed soft sensors for multiplex sensing of hemodynamics. *Sci Adv*. 2022;8:eabm1175. <https://doi.org/10.1126/sciadv.abm1175>.
- Papay P, Ignjatovic A, Karmiris K, et al. Optimising monitoring in the management of Crohn's disease: A physician's perspective. *Journal of Crohn's and Colitis*. 2013;7:653–69. <https://doi.org/10.1016/j.crohns.2013.02.005>.
- Madhvapathy SR, Bury MI, Wang LW, et al. Miniaturized implantable temperature sensors for the long-term monitoring of chronic intestinal inflammation. *Nat Biomed Eng*. 2024;8:1040. <https://doi.org/10.1038/s41551-024-01183-w>.
- Lin J, Chen X, Zhang P, et al. Wireless bioelectronics for in vivo pressure monitoring with mechanically-compliant hydrogel biointerfaces. *Adv Mater*. 2024;36:2400181. <https://doi.org/10.1002/adma.202400181>.

24. Herbert R, Elsisy M, Rigo B, et al. Fully implantable batteryless soft platforms with printed nanomaterial-based arterial stiffness sensors for wireless continuous monitoring of restenosis in real time. *Nano Today*. 2022;46: 101557. <https://doi.org/10.1016/j.nantod.2022.101557>.
25. Sheng F, Zhang B, Zhang Y, et al. Ultrastretchable organogel/silicone fiber-helical sensors for self-powered implantable ligament strain monitoring. *ACS Nano*. 2022;16:10958–67. <https://doi.org/10.1021/acsnano.2c03365>.
26. Noma H, Hasegawa Y, Matsushima M, et al. Micro-machined stent flow sensor for detecting breathing and heartbeat from air-flow in airway of rat. *J Micromech Microeng*. 2020;31: 025006. <https://doi.org/10.1088/1361-6439/abd07a>.
27. Cai L, Burton A, Gonzales DA, et al. Osseosurface electronics—thin, wireless, battery-free and multimodal musculoskeletal biointerfaces. *Nat Commun*. 2021;12:6707. <https://doi.org/10.1038/s41467-021-27003-2>.
28. Hench LL. 8 - The skeletal system. In: Hench LL, Jones JR (eds) *Biomaterials, artificial organs and tissue engineering*. Cambridge: Woodhead Publishing; 2005, pp 79–89. <https://doi.org/10.1533/9781845690861.2.79>.
29. Protti A, Cressoni M, Santini A, et al. Lung stress and strain during mechanical ventilation. *Am J Respir Crit Care Med*. 2011;183:1354–62. <https://doi.org/10.1164/rccm.201010-1757OC>.
30. Brady B, King G, Murphy RT, Walsh D. Myocardial strain: a clinical review. *Ir J Med Sci*. 2022; 1–8. <https://doi.org/10.1007/s11845-022-03210-8>
31. Schmidt P, Lestrup C, Thorning M, et al. Speckle tracking ultrasonography for assessment of skeletal muscle strain in m. soleus. A validity and reliability study on healthy participants. *Gait Posture*. 2020;81:333–4. <https://doi.org/10.1016/j.gaitpost.2020.08.063>.
32. Gilja OH, Heimdal A, Hausken T, et al. Strain during gastric contractions can be measured using Doppler ultrasonography. *Ultrasound Med Biol*. 2002;28:1457–65. [https://doi.org/10.1016/S0301-5629\(02\)00614-2](https://doi.org/10.1016/S0301-5629(02)00614-2).
33. Emig R, Zgierski-Johnston CM, Timmermann V, et al. Passive myocardial mechanical properties: meaning, measurement, models. *Biophys Rev*. 2021;13:587–610. <https://doi.org/10.1007/s12551-021-00838-1>.
34. Gotti C, Sensini A, Zucchelli A, et al. Hierarchical fibrous structures for muscle-inspired soft-actuators: A review. *Appl Mater Today*. 2020;20: 100772. <https://doi.org/10.1016/j.apmt.2020.100772>.
35. Gao F, Guo Z, Sakamoto M, Matsuzawa T. Fluid-structure interaction within a layered aortic arch model. *J Biol Phys*. 2006;32:435–54. <https://doi.org/10.1007/s10867-006-9027-7>.
36. Karatolios K, Wittek A, Nwe TH, et al. Method for aortic wall strain measurement with three-dimensional ultrasound speckle tracking and fitted finite element analysis. *Ann Thorac Surg*. 2013;96:1664–71. <https://doi.org/10.1016/j.athoracsur.2013.06.037>.
37. Kharazi M, Bohm S, Theodorakis C, et al. Quantifying mechanical loading and elastic strain energy of the human Achilles tendon during walking and running. *Sci Rep*. 2021;11:5830. <https://doi.org/10.1038/s41598-021-84847-w>.
38. Lim Y, Deo D, Singh TP, et al. In situ measurement and modeling of biomechanical response of human cadaveric soft tissues for physics-based surgical simulation. *Surg Endosc*. 2009;23:1298–307. <https://doi.org/10.1007/s00464-008-0154-z>.
39. Bin Y, Oishi K, Yoshida K, Matsuo M. Mechanical properties of poly(ethylene terephthalate) estimated in terms of orientation distribution of crystallites and amorphous chain segments under simultaneous biaxially stretching. *Polym J*. 2004;36:888–98. <https://doi.org/10.1295/polymj.36.888>.
40. Jain N, Singh VK, Chauhan S. A review on mechanical and water absorption properties of polyvinyl alcohol based composites/films. *J Mech Behav Mater*. 2017;26:213–22. <https://doi.org/10.1515/jmbm-2017-0027>.
41. Niu H, Wang H, Zhou H, Lin T. Ultrafine PDMS fibers: preparation from in situ curing-electrospinning and mechanical characterization. *RSC Adv*. 2014;4:11782–7. <https://doi.org/10.1039/C4RA00232F>.
42. Markert CD, Guo X, Skardal A, et al. Characterizing the micro-scale elastic modulus of hydrogels for use in regenerative medicine. *J Mech Behav Biomed Mater*. 2013;27:115–27. <https://doi.org/10.1016/j.jmbbm.2013.07.008>.
43. Banerjee A, Arha M, Choudhary S, et al. The influence of hydrogel modulus on the proliferation and differentiation of encapsulated neural stem cells. *Biomaterials*. 2009;30:4695–9. <https://doi.org/10.1016/j.biomaterials.2009.05.050>.
44. Papani R, Li Y, Wang S. Soft mechanical sensors for wearable and implantable applications. *WIREs Nanomed Nanobiotechnol*. 2024;16: e1961. <https://doi.org/10.1002/wnan.1961>.
45. Guimarães CF, Gasperini L, Marques AP, Reis RL. The stiffness of living tissues and its implications for tissue engineering. *Nat Rev Mater*. 2020;5:351–70. <https://doi.org/10.1038/s41578-019-0169-1>.
46. Tang H, Yang Y, Liu Z, et al. Injectable ultrasonic sensor for wireless monitoring of intracranial signals. *Nature*. 2024;630:84–90. <https://doi.org/10.1038/s41586-024-07334-y>.
47. Oh B, Lim Y-S, Ko KW, et al. Ultra-soft and highly stretchable tissue-adhesive hydrogel based multifunctional implantable sensor for monitoring of overactive bladder. *Biosens Bioelectron*. 2023;225: 115060. <https://doi.org/10.1016/j.bios.2023.115060>.
48. Burton AR, Sun P, Lynch JP. Bio-compatible wireless inductive thin-film strain sensor for monitoring the growth and strain response of bone in osseointegrated prostheses. *Struct Health Monit*. 2021;20:749–67. <https://doi.org/10.1177/1475921719831452>.
49. Souri H, Banerjee H, Jusufi A, et al. Wearable and stretchable strain sensors: materials, sensing mechanisms, and applications. *Adv Intell Syst*. 2020;2:2000039. <https://doi.org/10.1002/aisy.202000039>.
50. Fleming BC, Beynon BD. In vivo measurement of ligament/tendon strains and forces: a review. *Ann Biomed Eng*. 2004;32:318–28. <https://doi.org/10.1023/B:ABME.0000017542.75080.86>.
51. Wang K, Mak C-H, Ho JDL, et al. Large-scale surface shape sensing with learning-based computational mechanics. *Adv Intell Syst*. 2021;3:2100089. <https://doi.org/10.1002/aisy.202100089>.
52. Guo J, Niu M, Yang C. Highly flexible and stretchable optical strain sensing for human motion detection. *Optica, OPTICA*. 2017;4:1285–8. <https://doi.org/10.1364/OPTICA.4.001285>.
53. Khan A, Joshi R, Sharma MK, et al. Piezoelectric and triboelectric nanogenerators: Promising technologies for self-powered implantable biomedical devices. *Nano Energy*. 2024;119: 109051. <https://doi.org/10.1016/j.nanoen.2023.109051>.
54. Kim Y-G, Song J-H, Hong S, Ahn S-H. Piezoelectric strain sensor with high sensitivity and high stretchability based on kirigami design cutting. *Npj Flex Electron*. 2022;6:1–8. <https://doi.org/10.1038/s41528-022-00186-4>.
55. Ma Y, Zheng Q, Liu Y, et al. Self-powered, one-stop, and multifunctional implantable triboelectric active sensor for real-time biomedical monitoring. *Nano Lett*. 2016;16:6042–51. <https://doi.org/10.1021/acs.nanolett.6b01968>.
56. Ramanathan AK, Headings LM, Dapino MJ. Near static strain measurement with piezoelectric films. *Sens Actuator A-Phys*. 2020;301: 111654. <https://doi.org/10.1016/j.sna.2019.111654>.
57. Won SM, Wang H, Kim BH, et al. Multimodal sensing with a three-dimensional piezoresistive structure. *ACS Nano*. 2019;13:10972–9. <https://doi.org/10.1021/acsnano.9b02030>.

58. Lee JH, Kim SH, Heo JS, et al. Heterogeneous structure omnidirectional strain sensor arrays with cognitively learned neural networks. *Adv Mater.* 2023;35:2208184. <https://doi.org/10.1002/adma.202208184>.
59. Duan Z, Yuan M, Liu Z, et al. An ultrasensitive $Ti_3C_2T_x$ Mxene-based soft contact lens for continuous and nondestructive intraocular pressure monitoring. *Small.* 2024; n/a:2309785. <https://doi.org/10.1002/smll.202309785>
60. Na HR, Lee HJ, Jeon JH, et al. Vertical graphene on flexible substrate, overcoming limits of crack-based resistive strain sensors. *Npj Flex Electron.* 2022;6:1–8. <https://doi.org/10.1038/s41528-022-00135-1>.
61. Chen J, Zhang J, Luo Z, et al. Superelastic, sensitive, and low hysteresis flexible strain sensor based on wave-patterned liquid metal for human activity monitoring. *ACS Appl Mater Interfaces.* 2020;12:22200–11. <https://doi.org/10.1021/acsami.0c04709>.
62. Wu S, Kim D, Tang X, et al. Encapsulated stretchable amphibious strain sensors. *Mater Horiz.* <https://doi.org/10.1039/D4MH00757C>
63. Derenzo SE. Practical strain gage measurement. In: *Interfacing: a laboratory approach using the microcomputer for instrumentation, data analysis, and control.* Englewood Cliffs, N.J. : Prentice Hall, p pp 169–170
64. Jin L, Chortos A, Lian F, et al. Microstructural origin of resistance–strain hysteresis in carbon nanotube thin film conductors. *Proc Natl Acad Sci USA.* 2018;115:1986–91. <https://doi.org/10.1073/pnas.1717217115>.
65. Zhang D, Zhang J, Wu Y, et al. Liquid metal interdigitated capacitive strain sensor with normal stress insensitivity. *Adv Intell Syst.* 2022;4:2100201. <https://doi.org/10.1002/aisy.202100201>.
66. Cai L, Song L, Luan P, et al. Super-stretchable, transparent carbon nanotube-based capacitive strain sensors for human motion detection. *Sci Rep.* 2013;3:3048. <https://doi.org/10.1038/srep03048>.
67. Frutiger A, Muth JT, Vogt DM, et al. Capacitive soft strain sensors via multicore–shell fiber printing. *Adv Mater.* 2015;27:2440–6. <https://doi.org/10.1002/adma.201500072>.
68. Shen Z, Liu F, Huang S, et al. Progress of flexible strain sensors for physiological signal monitoring. *Biosens Bioelectron.* 2022;211: 114298. <https://doi.org/10.1016/j.bios.2022.114298>.
69. Kim J, Bury MI, Kwon K, et al. A wireless, implantable bioelectronic system for monitoring urinary bladder function following surgical recovery. *Proc Natl Acad Sci USA.* 2024;121: e2400868121. <https://doi.org/10.1073/pnas.2400868121>.
70. Dual SA, Llerena Zambrano B, Sündermann S, et al. Continuous heart volume monitoring by fully implantable soft strain sensor. *Adv Healthcare Mater.* 2020;9:2000855. <https://doi.org/10.1002/adhm.202000855>.
71. Hong W, Jiang C, Qin M, et al. Self-adaptive cardiac optogenetics device based on negative stretching-resistive strain sensor. *Sci Adv.* 2021;7:eabj4273. <https://doi.org/10.1126/sciadv.abj4273>.
72. Lee J, Ihle SJ, Pellegrino GS, et al. Stretchable and suturable fibre sensors for wireless monitoring of connective tissue strain. *Nat Electron.* 2021;4:291–301. <https://doi.org/10.1038/s41928-021-00557-1>.
73. Zhang Q, Bossuyt FM, Adam NC, et al. A stretchable strain sensor system for wireless measurement of musculoskeletal soft tissue strains. *Adv Mater Technol.* 2023;8:2202041. <https://doi.org/10.1002/admt.202202041>.
74. Zhang Y, Cui J, Chen K-Y, et al. A smart coating with integrated physical antimicrobial and strain-mapping functionalities for orthopedic implants. *Sci Adv.* 2023;9:eadg7397. <https://doi.org/10.1126/sciadv.adg7397>.
75. Klosterhoff BS, Ghee Ong K, Krishnan L, et al. Wireless implantable sensor for noninvasive, longitudinal quantification of axial strain across rodent long bone defects. *J Biomech Eng.* 2017;139:1110041. <https://doi.org/10.1115/1.4037937>.
76. Huang X, Liu L, Lin YH, et al. High-stretchability and low-hysteresis strain sensors using origami-inspired 3D mesostructures. *Sci Adv.* 2023;9:eadh9799. <https://doi.org/10.1126/sciadv.adh9799>.
77. Lee JH, Jang T-M, Shin J-W, et al. Wireless, fully implantable and expandable electronic system for bidirectional electrical neuromodulation of the urinary bladder. *ACS Nano.* 2023;17:8511–20. <https://doi.org/10.1021/acsnano.3c00755>.
78. Arab Hassani F, Jin H, Yokota T, et al. Soft sensors for a sensing-actuation system with high bladder voiding efficiency. *Sci Adv.* 2020;6:eaba0412. <https://doi.org/10.1126/sciadv.aba0412>.
79. Yan D, Bruns TM, Wu Y, et al. Ultracompliant carbon nanotube direct bladder device. *Adv Healthcare Mater.* 2019;8:1900477. <https://doi.org/10.1002/adhm.201900477>.
80. Lee HJ, Ryu B, Lee DK, et al. Biocompatible cracked reduced graphene oxide strain sensors: enhancing implantable strain sensing performance and durability. *J Mater Chem C.* 2023;11:8405–12. <https://doi.org/10.1039/D3TC01266B>.
81. Ryu B, Kim C-Y, Park S-P, et al. In vivo implantable strain sensor for real-time and precise pathophysiological monitoring of contractile living organs. *Adv Func Mater.* 2023;33:2305769. <https://doi.org/10.1002/adfm.202305769>.
82. Semproni F, Iacovacci V, Menciassi A. Bladder monitoring systems: state of the art and future perspectives. *IEEE Access.* 2022;10:125626–51. <https://doi.org/10.1109/ACCESS.2022.3221816>.
83. Hakenberg OW, Linne C, Manseck A, Wirth MP. Bladder wall thickness in normal adults and men with mild lower urinary tract symptoms and benign prostatic enlargement. *Neurourol Urodyn.* 2000;19:585–93. [https://doi.org/10.1002/1520-6777\(2000\)19:5%3c585::AID-NAU5%3e3.0.CO;2-U](https://doi.org/10.1002/1520-6777(2000)19:5%3c585::AID-NAU5%3e3.0.CO;2-U).
84. Mickle AD, Won SM, Noh KN, et al. A wireless closed-loop system for optogenetic peripheral neuromodulation. *Nature.* 2019;565:361–5. <https://doi.org/10.1038/s41586-018-0823-6>.
85. Pastena P, Frye JT, Ho C, et al. Ischemic cardiomyopathy: epidemiology, pathophysiology, outcomes, and therapeutic options. *Heart Fail Rev.* 2024;29:287–99. <https://doi.org/10.1007/s10741-023-10377-4>.
86. Luis SA, Chan J, Pellikka PA. Echocardiographic assessment of left ventricular systolic function: an overview of contemporary techniques, including speckle-tracking echocardiography. *Mayo Clin Proc.* 2019;94:125–38. <https://doi.org/10.1016/j.mayocp.2018.07.017>.
87. Hoit BD. Normal cardiac physiology and ventricular function. In: *Reference module in biomedical sciences.* 3rd ed. Elsevier. 2014. <https://doi.org/10.1016/B978-0-12-801238-3.00197-5>.
88. Elaskalany M, Behdinin K. Effect of carbon nanotube type and length on the electrical conductivity of carbon nanotube polymer nanocomposites. *Mater Res Express.* 2023;10: 105010. <https://doi.org/10.1088/2053-1591/ad0440>.
89. Entcheva E, Kay MW. Cardiac optogenetics: a decade of enlightenment. *Nat Rev Cardiol.* 2021;18:349–67. <https://doi.org/10.1038/s41569-020-00478-0>.
90. Xia Y, Zhang Q, Wu XE, et al. Practical and durable flexible strain sensors based on conductive carbon black and silicone blends for large scale motion monitoring applications. *Sensors.* 2019;19:4553. <https://doi.org/10.3390/s19204553>.
91. Yao S, Vargas L, Hu X, Zhu Y. A novel finger kinematic tracking method based on skin-like wearable strain sensors. *IEEE Sens J.* 2018;18:3010–5. <https://doi.org/10.1109/JSEN.2018.2802421>.
92. James R, Kesturu G, Balian G, Chhabra AB. Tendon: biology, biomechanics, repair, growth factors, and evolving treatment

- options. *J Hand Surg.* 2008;33:102–12. <https://doi.org/10.1016/j.jhsa.2007.09.007>.
93. Almansoori MT, Li X, Zheng L. A brief review on e-skin and its multifunctional sensing applications. *Curr Smart Mater.* 2019;4:3–14. <https://doi.org/10.2174/2405465804666190313154903>.
 94. Zhang Q, Adam NC, Hosseini Nasab SH, et al. Techniques for in vivo measurement of ligament and tendon strain: a review. *Ann Biomed Eng.* 2021;49:7–28. <https://doi.org/10.1007/s10439-020-02635-5>.
 95. Adam NC, Smith CR, Herzog W, et al. In vivo strain patterns in the achilles tendon during dynamic activities: a comprehensive survey of the literature. *Sports Med Open.* 2023;9:60. <https://doi.org/10.1186/s40798-023-00604-5>.
 96. Beynon BD, Fleming BC. Anterior cruciate ligament strain in vivo: a review of previous work. *J Biomech.* 1998;31:519–25. [https://doi.org/10.1016/S0021-9290\(98\)00044-X](https://doi.org/10.1016/S0021-9290(98)00044-X).
 97. Boutry CM, Kaizawa Y, Schroeder BC, et al. A stretchable and biodegradable strain and pressure sensor for orthopaedic application. *Nat Electron.* 2018;1:314–21. <https://doi.org/10.1038/s41928-018-0071-7>.
 98. Yogev D, Goldberg T, Arami A, et al. Current state of the art and future directions for implantable sensors in medical technology: Clinical needs and engineering challenges. *APL Bioeng.* 2023;7:031506. <https://doi.org/10.1063/5.0152290>.
 99. Nelson BD, Karipott SS, Wang Y, Ong KG. Wireless technologies for implantable devices. *Sensors.* 2020;20:4604. <https://doi.org/10.3390/s20164604>.
 100. Steinmann S, Pfeifer CG, Brochhausen C, Docheva D. Spectrum of tendon pathologies: triggers, trails and end-state. *Int J Mol Sci.* 2020;21:844. <https://doi.org/10.3390/ijms21030844>.
 101. Wu F, Nerlich M, Docheva D. Tendon injuries: basic science and new repair proposals. *EFORT Open Reviews.* 2017;2:332–42. <https://doi.org/10.1302/2058-5241.2.160075>.
 102. Iwanuma S, Akagi R, Kurihara T, et al. Longitudinal and transverse deformation of human Achilles tendon induced by isometric plantar flexion at different intensities. *J Appl Physiol.* 2011;110:1615–21. <https://doi.org/10.1152/jappphysiol.00776.2010>.
 103. Waugh CM, Blazeovich AJ, Fath F, Korff T. Age-related changes in mechanical properties of the Achilles tendon. *J Anat.* 2012;220:144–55. <https://doi.org/10.1111/j.1469-7580.2011.01461.x>.
 104. Erdemir A, Hamel AJ, Piazza SJ, Sharkey NA. Fiberoptic measurement of tendon forces is influenced by skin movement artifact. *J Biomech.* 2003;36:449–55. [https://doi.org/10.1016/S0021-9290\(02\)00414-1](https://doi.org/10.1016/S0021-9290(02)00414-1).
 105. Asahara H, Inui M, Lotz MK. Tendons and ligaments: connecting developmental biology to musculoskeletal disease pathogenesis. *J Bone Miner Res.* 2017;32:1773–82. <https://doi.org/10.1002/jbmr.3199>.
 106. Mintz EL, Passipieri JA, Franklin IR, et al. Long-term evaluation of functional outcomes following rat volumetric muscle loss injury and repair. *Tissue Eng Part A.* 2020;26:140–56. <https://doi.org/10.1089/ten.tea.2019.0126>.
 107. Kim T, See CW, Li X, Zhu D. Orthopedic implants and devices for bone fractures and defects: Past, present and perspective. *Eng Regen.* 2020;1:6–18. <https://doi.org/10.1016/j.engreg.2020.05.003>.
 108. Szivek JA, Roberto RF, Margolis DS. In vivo strain measurements from hardware and lamina during spine fusion. *J Biomed Mater Res Part B.* 2005;75B:243–50. <https://doi.org/10.1002/jbm.b.30262>.
 109. Dall'Ara E, Barber D, Viceconti M. About the inevitable compromise between spatial resolution and accuracy of strain measurement for bone tissue: a 3D zero-strain study. *J Biomech.* 2014;47:2956–63. <https://doi.org/10.1016/j.jbiomech.2014.07.019>.
 110. Wu A-M, Bisignano C, James SL, et al. Global, regional, and national burden of bone fractures in 204 countries and territories, 1990–2019: a systematic analysis from the Global Burden of Disease Study 2019. *The Lancet Healthy Longevity.* 2021;2:e580–92. [https://doi.org/10.1016/S2666-7568\(21\)00172-0](https://doi.org/10.1016/S2666-7568(21)00172-0).
 111. Sharif-Alhoseini M, Khormali M, Rezaei M, et al. Animal models of spinal cord injury: a systematic review. *Spinal Cord.* 2017;55:714–21. <https://doi.org/10.1038/sc.2016.187>.
 112. Shi Y, Tang S, Zhang W, et al. A reliable, battery-free and implantable magnetic sensing system for wireless monitoring of spinal motion in rats and humans. *Chem Eng J.* 2024;482:148891. <https://doi.org/10.1016/j.cej.2024.148891>.
 113. Al-Shalawi FD, Mohamed Ariff AH, Jung D-W, et al. Biomaterials as implants in the orthopedic field for regenerative medicine: metal versus synthetic polymers. *Polymers.* 2023;15:2601. <https://doi.org/10.3390/polym15122601>.
 114. Vining KH, Mooney DJ. Mechanical forces direct stem cell behaviour in development and regeneration. *Nat Rev Mol Cell Biol.* 2017;18:728–42. <https://doi.org/10.1038/nrm.2017.108>.
 115. McDermott AM, Herberg S, Mason DE, et al. Recapitulating bone development through engineered mesenchymal condensations and mechanical cues for tissue regeneration. *Sci Transl Med.* 2019;11:eaav7756. <https://doi.org/10.1126/scitranslmed.aav7756>.
 116. Rot C, Stern T, Blecher R, et al. A mechanical jack-like mechanism drives spontaneous fracture healing in neonatal mice. *Dev Cell.* 2014;31:159–70. <https://doi.org/10.1016/j.devcel.2014.08.026>.
 117. Klosterhoff BS, Kaiser J, Nelson BD, et al. Wireless sensor enables longitudinal monitoring of regenerative niche mechanics during rehabilitation that enhance bone repair. *Bone.* 2020;135:115311. <https://doi.org/10.1016/j.bone.2020.115311>.
 118. Yang J, Luo S, Zhou X, et al. Flexible, tunable, and ultrasensitive capacitive pressure sensor with microconformal graphene electrodes. *ACS Appl Mater Interfaces.* 2019;11:14997–5006. <https://doi.org/10.1021/acsami.9b02049>.
 119. Sun J, Guo H, Ribera J, et al. Sustainable and biodegradable wood sponge piezoelectric nanogenerator for sensing and energy harvesting applications. *ACS Nano.* 2020;14:14665–74. <https://doi.org/10.1021/acs.nano.0c05493>.
 120. Shin J, Liu Z, Bai W, et al. Bioresorbable optical sensor systems for monitoring of intracranial pressure and temperature. *Sci Adv.* 2019;5:eaaw1899. <https://doi.org/10.1126/sciadv.aaw1899>.
 121. Xu K, Li S, Dong S, et al. Bioresorbable electrode array for electrophysiological and pressure signal recording in the brain. *Adv Healthcare Mater.* 2019;8:1801649. <https://doi.org/10.1002/adhm.201801649>.
 122. Lu D, Yan Y, Deng Y, et al. Bioresorbable wireless sensors as temporary implants for in vivo measurements of pressure. *Adv Funct Mater.* 2020;30:2003754. <https://doi.org/10.1002/adfm.202003754>.
 123. Hu S, Chen H, Jia S, et al. A wireless passive extra-arterial implantable blood pressure monitoring sensing system for rats. *Microsyst Technol.* 2021;27:2595–603. <https://doi.org/10.1007/s00542-020-05011-4>.
 124. Oyunbaatar N-E, Kim D-S, Shanmugasundaram A, et al. Implantable self-reporting stents for detecting in-stent restenosis and cardiac functional dynamics. *ACS Sens.* 2023;8:4542–53. <https://doi.org/10.1021/acssensors.3c01313>.
 125. Magkoutas K, Weisskopf M, Falk V, et al. Continuous monitoring of blood pressure and vascular hemodynamic properties with miniature extravascular hall-based magnetic sensor. *J Am Coll Cardiol Basic Trans Science.* 2023;8:546–64. <https://doi.org/10.1016/j.jacbs.2022.12.008>.

126. Ouyang H, Li Z, Gu M, et al. A bioresorbable dynamic pressure sensor for cardiovascular postoperative care. *Adv Mater*. 2021;33:2102302. <https://doi.org/10.1002/adma.202102302>.
127. Raboel PH, Bartek J, Andresen M, et al. Intracranial pressure monitoring: invasive versus non-invasive methods—a review. *Crit Care Res Pract*. 2012;2012:1–14. <https://doi.org/10.1155/2012/950393>.
128. Su S-H, Wang F, Hai J, et al. The effects of intracranial pressure monitoring in patients with traumatic brain injury. *PLoS ONE*. 2014;9: e87432. <https://doi.org/10.1371/journal.pone.0087432>.
129. Miller JD, Becker DP, Ward JD, et al. Significance of intracranial hypertension in severe head injury. *J Neurosurg*. 1977;47:503–16. <https://doi.org/10.3171/jns.1977.47.4.503>.
130. Stehlin E, Malpas S, Heppner P, et al. Implantable ICP monitor for improved hydrocephalus management. In: Schuhmann MU, Czosnyka M (eds) *Intracranial Pressure and Brain Monitoring XIV*. Springer Vienna, Vienna, pp 101–104
131. Zacchetti L, Magnoni S, Di Corte F, et al. Accuracy of intracranial pressure monitoring: systematic review and meta-analysis. *Crit Care*. 2015;19:420. <https://doi.org/10.1186/s13054-015-1137-9>.
132. Padayachy LC, Figaji AA, Bullock MR. Intracranial pressure monitoring for traumatic brain injury in the modern era. *Childs Nerv Syst*. 2010;26:441–52. <https://doi.org/10.1007/s00381-009-1034-0>.
133. De Laet I, Citerio G, Malbrain MLNG. The influence of intra-abdominal hypertension on the central nervous system: current insights and clinical recommendations, is it all in the head? *Acta Clin Belg*. 2007;62:89–97. <https://doi.org/10.1179/acb.2007.62.s1.012>.
134. Bothwell SW, Janigro D, Patabendige A. Cerebrospinal fluid dynamics and intracranial pressure elevation in neurological diseases. *Fluids Barriers CNS*. 2019;16:9. <https://doi.org/10.1186/s12987-019-0129-6>.
135. Munakomi S, Das JM. *Intracranial pressure monitoring*. In: StatPearls. Treasure Island: StatPearls Publishing; 2024. <http://www.ncbi.nlm.nih.gov/books/NBK542298/>.
136. Steiner LA, Andrews PJD. Monitoring the injured brain: ICP and CBF. *Br J Anaesth*. 2006;97:26–38. <https://doi.org/10.1093/bja/ael110>.
137. Czosnyka M, Pickard JD. Monitoring and interpretation of intracranial pressure. *J Neurol Neurosurg Psychiatry*. 2004;75:813. <https://doi.org/10.1136/jnnp.2003.033126>.
138. Malbrain MLNG, Cheatham ML, Kirkpatrick A, et al. Results from the international conference of experts on intra-abdominal hypertension and abdominal compartment syndrome. I Definitions *Intensive Care Med*. 2006;32:1722–32. <https://doi.org/10.1007/s00134-006-0349-5>.
139. Authors/Task Force Members, Galie N, Hoeper MM, et al. Guidelines for the diagnosis and treatment of pulmonary hypertension: the task force for the diagnosis and treatment of pulmonary hypertension of the European Society of Cardiology (ESC) and the European Respiratory Society (ERS), endorsed by the International Society of Heart and Lung Transplantation (ISHLT). *European Heart J*. 2009;30:2493–537. <https://doi.org/10.1093/eurheartj/ehp297>.
140. World Health Organization. *Noncommunicable diseases country profiles 2018*. World Health Organization, Geneva
141. Zhang C, Ouyang W, Zhang L, Li D. A dual-mode fiber-shaped flexible capacitive strain sensor fabricated by direct ink writing technology for wearable and implantable health monitoring applications. *Microsyst Nanoeng*. 2023;9:158. <https://doi.org/10.1038/s41378-023-00634-9>.
142. Sheridan WS, Wetterling F, Testani JM, et al. Safety and performance of a novel implantable sensor in the inferior vena cava under acute and chronic intravascular volume modulation. *Eur J Heart Fail*. 2023;25:754–63. <https://doi.org/10.1002/ejhf.2822>.
143. Omar R, Saliba W, Khatib M, et al. Biodegradable, biocompatible, and implantable multifunctional sensing platform for cardiac monitoring. *ACS Sens*. 2024;9:126–38. <https://doi.org/10.1021/acssensors.3c01755>.
144. Kwak BR, Bäck M, Bochaton-Piallat M-L, et al. Biomechanical factors in atherosclerosis: mechanisms and clinical implications. *Eur Heart J*. 2014;35:3013–20. <https://doi.org/10.1093/eurheartj/ehu353>.
145. Virani SS, Alonso A, Benjamin EJ, et al. Heart disease and stroke statistics—2020 update: a report from the american heart association. *Circulation*. 2020;141:e139–596. <https://doi.org/10.1161/CIR.0000000000000757>.
146. Herbert R, Mishra S, Lim H, et al. Fully printed, wireless, stretchable implantable biosystem toward batteryless, real-time monitoring of cerebral aneurysm hemodynamics. *Adv Sci*. 2019;6:1901034. <https://doi.org/10.1002/adv.201901034>.
147. Huygh J, Peeters Y, Bernards J, Malbrain MLNG. Hemodynamic monitoring in the critically ill: an overview of current cardiac output monitoring methods. *F1000Res*. 2016; 5:F1000 Faculty Rev-2855. <https://doi.org/10.12688/f1000research.8991.1>
148. Couture EJ, Laferrière-Langlois P, Denault A. New developments in continuous hemodynamic monitoring of the critically ill patient. *Can J Cardiol*. 2023;39:432–43. <https://doi.org/10.1016/j.cjca.2023.01.012>.
149. Dai J, Li L, Shi B, Li Z. Recent progress of self-powered respiration monitoring systems. *Biosens and Bioelectron*. 2021;194: 113609. <https://doi.org/10.1016/j.bios.2021.113609>.
150. Hussain T, Ullah S, Fernández-García R, Gil I. Wearable sensors for respiration monitoring: a review. *Sensors*. 2023;23:7518. <https://doi.org/10.3390/s23177518>.
151. Kwon K, Kim JU, Won SM, et al. A battery-less wireless implant for the continuous monitoring of vascular pressure, flow rate and temperature. *Nat Biomed Eng*. 2023;7:1215–28. <https://doi.org/10.1038/s41551-023-01022-4>.
152. Lu D, Li S, Yang Q, et al. Implantable, wireless, self-fixing thermal sensors for continuous measurements of microvascular blood flow in flaps and organ grafts. *Biosens Bioelectron*. 2022;206: 114145. <https://doi.org/10.1016/j.bios.2022.114145>.
153. Maeda Y, Okihara C, Hasegawa Y, et al. Catheter sensor system for in-situ breathing and optical imaging measurements at airway in inside of lung. *Microsyst Technol*. 2020;26:3705–13. <https://doi.org/10.1007/s00542-020-04843-4>.
154. Smith SA, Travers RJ, Morrissey JH. How it all starts: initiation of the clotting cascade. *Crit Rev Biochem Mol Biol*. 2015;50:326–36. <https://doi.org/10.3109/10409238.2015.1050550>.
155. Pareja E, Cortes M, Navarro R, et al. Vascular complications after orthotopic liver transplantation: hepatic artery thrombosis. *Transplant Proc*. 2010;42:2970–2. <https://doi.org/10.1016/j.transproceed.2010.07.063>.
156. Cheong JH, Ng SSY, Liu X, et al. An inductively powered implantable blood flow sensor microsystem for vascular grafts. *IEEE Trans Biomed Eng*. 2012;59:2466–75. <https://doi.org/10.1109/TBME.2012.2203131>.
157. Rosenthal G, Sanchez-Mejia RO, Phan N, et al. Incorporating a parenchymal thermal diffusion cerebral blood flow probe in bedside assessment of cerebral autoregulation and vasoreactivity in patients with severe traumatic brain injury. *J Neurosurg*. 2011;114:62–70. <https://doi.org/10.3171/2010.6.JNS091360>.
158. King LV. On the convection of heat from small cylinders in a stream of fluid: determination of the convection constants of small platinum wires, with applications to hot-wire anemometry. *Proc R Soc London, Ser A*. 1914;90:563–70. <https://doi.org/10.1098/rspa.1914.0089>.

159. Tan CL, Knight ZA. Regulation of body temperature by the nervous system. *Neuron*. 2018;98:31–48. <https://doi.org/10.1016/j.neuron.2018.02.022>.
160. Chanmugam A, Langemo D, Thomason K, et al. Relative temperature maximum in wound infection and inflammation as compared with a control subject using long-wave infrared thermography. *Adv Skin Wound Care*. 2017;30:406–14. <https://doi.org/10.1097/01.ASW.0000522161.13573.62>.
161. Reverter F. A tutorial on thermal sensors in the 200th anniversary of the seebeck effect. *IEEE Sensors J*. 2021;21:22122–32. <https://doi.org/10.1109/JSEN.2021.3105546>.
162. Chen X, Park YJ, Kang M, et al. CVD-grown monolayer MoS₂ in bioabsorbable electronics and biosensors. *Nat Commun*. 2018;9:1–12. <https://doi.org/10.1038/s41467-018-03956-9>.
163. Bajzek TJ. Thermocouples: a sensor for measuring temperature. *IEEE Instrum Meas Mag*. 2005;8:35–40. <https://doi.org/10.1109/MIM.2005.1405922>.
164. Sahasrabudhe A, Rupprecht LE, Orguc S, et al. Multifunctional microelectronic fibers enable wireless modulation of gut and brain neural circuits. *Nat Biotechnol*. 2024;42:892. <https://doi.org/10.1038/s41587-023-01833-5>.
165. Lu D, Yan Y, Avila R, et al. Bioresorbable, wireless, passive sensors as temporary implants for monitoring regional body temperature. *Adv Healthcare Mater*. 2020;9:2000942. <https://doi.org/10.1002/adhm.202000942>.
166. Webb RC, Bonifas AP, Behnaz A, et al. Ultrathin conformal devices for precise and continuous thermal characterization of human skin. *Nature Mater*. 2013;12:938–44. <https://doi.org/10.1038/nmat3755>.
167. Uchida K, Takahashi S, Harii K, et al. Observation of the spin Seebeck effect. *Nature*. 2008;455:778–81. <https://doi.org/10.1038/nature07321>.
168. Wang J, Xie H, Chung T, et al. Neural probes with integrated temperature sensors for monitoring retina and brain implantation and stimulation. *IEEE Trans Neural Syst Rehabil Eng*. 2017;25:1663–73. <https://doi.org/10.1109/TNSRE.2016.2634584>.
169. Shi C, Andino-Pavlovsky V, Lee SA, et al. Application of a sub-0.1-mm³ implantable mote for in vivo real-time wireless temperature sensing. *Sci Adv*. 2021;7:eabf6312. <https://doi.org/10.1126/sciadv.abf6312>.
170. Shi C, Costa T, Elloian J, et al. A 0.065-mm³ monolithically-integrated ultrasonic wireless sensing mote for real-time physiological temperature monitoring. *IEEE Trans Biomed Circuits Syst*. 2020;14:412–24. <https://doi.org/10.1109/TBCAS.2020.2971066>.
171. Roda G, Chien Ng S, Kotze PG, et al. Crohn's disease *Nat Rev Dis Primers*. 2020;6:1–19. <https://doi.org/10.1038/s41572-020-0156-2>.
172. Chen S-L, Lundy DJ, Ruan S-C, et al. The gut microbiota regulates acute foreign body reaction and tissue repair after biomaterial implantation. *Biomaterials*. 2022;289: 121807. <https://doi.org/10.1016/j.biomaterials.2022.121807>.
173. Ellison GW, Case JB, Regier PJ. Intestinal surgery in small animals: historical foundations, current thinking, and future horizons. *Vet Surg*. 2019;48:1171–80. <https://doi.org/10.1111/vsu.13275>.
174. Xing L, Cheng Q, Zha G, Yi S. Transcriptional profiling at high temporal resolution reveals robust immune/inflammatory responses during rat sciatic nerve recovery. *Mediators Inflamm*. 2017;2017:1–7. <https://doi.org/10.1155/2017/3827841>.
175. Wysocki AB. Evaluating and managing open skin wounds: colonization versus infection. *AACN Clinical Issues: Advanced Practice in Acute and Critical Care*. 2002;13:382–97. <https://doi.org/10.1097/00044067-200208000-00005>.
176. Bakdash K, Schramm KM, Annam A, et al. Complications of percutaneous renal biopsy. *Semin Intervent Radiol*. 2019;36:097–103. <https://doi.org/10.1055/s-0039-1688422>.
177. Schnuelle P. Renal biopsy for diagnosis in kidney disease: indication, technique, and safety. *JCM*. 2023;12:6424. <https://doi.org/10.3390/jcm12196424>.
178. Edelstein CL. Biomarkers in acute kidney injury. In: *Biomarkers of kidney disease*. San Diego: Elsevier; 2017, pp 241–315. <https://doi.org/10.1016/B978-0-12-803014-1.00006-6>.
179. Kariyott SS, Veetil PM, Nelson BD, et al. An embedded wireless temperature sensor for orthopedic implants. *IEEE Sens J*. 2018;18:1265–72. <https://doi.org/10.1109/JSEN.2017.2780226>.
180. Maini L, Genovés V, Furrer R, et al. An in vitro demonstration of a passive, acoustic metamaterial as a temperature sensor with mK resolution for implantable applications. *Microsyst Nanoeng*. 2024;10:8. <https://doi.org/10.1038/s41378-023-00632-x>.
181. Liu CS, Rau A, Gallagher D, et al. Using transcranial direct current stimulation to treat symptoms in mild cognitive impairment and Alzheimer's disease. *Neurodegener Dis Manag*. 2017;7:317–29. <https://doi.org/10.2217/nmt-2017-0021>.
182. Cagnan H, Denison T, McIntyre C, Brown P. Emerging technologies for improved deep brain stimulation. *Nat Biotechnol*. 2019;37:1024–33. <https://doi.org/10.1038/s41587-019-0244-6>.
183. Cordaro NM, Szivek JA, DeYoung DW. Surface enhancements accelerate bone bonding to CPC-coated strain gauges. *J Biomed Mater Res*. 2001;56:109–19. [https://doi.org/10.1002/1097-4636\(200107\)56:1%3c109::AID-JBM1075%3e3.0.CO;2-W](https://doi.org/10.1002/1097-4636(200107)56:1%3c109::AID-JBM1075%3e3.0.CO;2-W).
184. Ed Margerrison, Argentieri M, Schoelles K, Lucas S. Medical device material performance study—poly lactic-co-glycolic acid [P (L/G) A] safety profile. In: *US FDA center for devices and radiological health*. <https://www.fda.gov/medical-devices/science-and-research-medical-devices/medical-device-material-safety-summaries>
185. Veronese FM, Pasut G. PEGylation, successful approach to drug delivery. *Drug Discovery Today*. 2005;10:1451–8. [https://doi.org/10.1016/S1359-6446\(05\)03575-0](https://doi.org/10.1016/S1359-6446(05)03575-0).
186. Jusu SM, Obayemi JD, Salifu AA, et al. Drug-encapsulated blend of PLGA-PEG microspheres: in vitro and in vivo study of the effects of localized/targeted drug delivery on the treatment of triple-negative breast cancer. *Sci Rep*. 2020;10:14188. <https://doi.org/10.1038/s41598-020-71129-0>.
187. López-Huerta F, Cervantes B, González O, et al. Biocompatibility and surface properties of tio2 thin films deposited by dc magnetron sputtering. *Materials*. 2014;7:4105–17. <https://doi.org/10.3390/ma7064105>.
188. Finch DS, Oreskovic T, Ramadurai K, et al. Biocompatibility of atomic layer-deposited alumina thin films. *J Biomedical Materials Res*. 2008;87A:100–6. <https://doi.org/10.1002/jbm.a.31732>.
189. Shi D, Narayanan S, Woepel K, Cui XT. Improving the biocompatibility and functionality of neural interface devices with silica nanoparticles. *Acc Chem Res*. 2024;57:1684–95. <https://doi.org/10.1021/acs.accounts.4c00160>.
190. Xuan L, Ju Z, Skonieczna M, et al. Nanoparticles-induced potential toxicity on human health: Applications, toxicity mechanisms, and evaluation models. *MedComm*. 2023;4: e327. <https://doi.org/10.1002/mco2.327>.
191. Matsuoka M, Akasaka T, Totsuka Y, Watari F. Carbon nanotube-coated silicone as a flexible and electrically conductive biomedical material. *Mater Sci Eng C*. 2012;32:574–80. <https://doi.org/10.1016/j.msec.2011.12.011>.
192. Mariello M, Kim K, Wu K, et al. Recent advances in encapsulation of flexible bioelectronic implants: materials, technologies, and characterization methods. *Adv Mater*. 2022;34:2201129. <https://doi.org/10.1002/adma.202201129>.

193. de Vries LM, Leening MJG, Dijk WA, et al. Trends in service time of pacemakers in the Netherlands: a long-term nationwide follow-up study. *Neth Heart J*. 2017;25:581–91. <https://doi.org/10.1007/s12471-017-1024-x>.
194. Truong T, Nguyen T, Zhao H, et al. Engineering stress in thin films: an innovative pathway toward 3D micro and nanosystems. *Small*. 2022;18:2105748. <https://doi.org/10.1002/sml.202105748>.
195. Jung D, Lim C, Shim HJ, et al. Highly conductive and elastic nanomembrane for skin electronics. *Science*. 2021;373:1022–6. <https://doi.org/10.1126/science.abh4357>.
196. Dickey MD. Stretchable and soft electronics using liquid metals. *Adv Mater*. 2017;29:1606425. <https://doi.org/10.1002/adma.201606425>.
197. Li X, Chen L, Yu G, et al. Rapid fabrication of high-resolution flexible electronics via nanoparticle self-assembly and transfer printing. *Nano Lett*. 2024; [acs.nanolett.3c04316](https://doi.org/10.1021/acs.nanolett.3c04316). <https://doi.org/10.1021/acs.nanolett.3c04316>
198. Zhao Q, Gribkova E, Shen Y, et al. Highly stretchable and customizable microneedle electrode arrays for intramuscular electromyography. *Sci Adv*. 2024;10:eadn7202. <https://doi.org/10.1126/sciadv.adn7202>.
199. Zhao H, Li K, Han M, et al. Buckling and twisting of advanced materials into morphable 3D mesostructures. *Proc Natl Acad Sci USA*. 2019;116:13239–48. <https://doi.org/10.1073/pnas.1901193116>.
200. Zhao H, Cheng X, Wu C, et al. Mechanically guided hierarchical assembly of 3D mesostructures. *Adv Mater*. 2022;34:2109416. <https://doi.org/10.1002/adma.202109416>.
201. Choi MK, Yang J, Kim DC, et al. Extremely vivid, highly transparent, and ultrathin quantum dot light-emitting diodes. *Adv Mater*. 2018;30:1703279. <https://doi.org/10.1002/adma.201703279>.
202. Jeong J, Chou N, Kim S. Long-term characterization of neural electrodes based on parylene-caulked polydimethylsiloxane substrate. *Biomed Microdevices*. 2016;18:42. <https://doi.org/10.1007/s10544-016-0065-z>.
203. Wu J, Yuk H, Sarrafian TL, et al. An off-the-shelf bioadhesive patch for sutureless repair of gastrointestinal defects. *Sci Transl Med*. 2022;14:eabh2857. <https://doi.org/10.1126/scitranslmed.abh2857>.
204. Zheng Y, Baidya A, Annabi N. Molecular design of an ultra-strong tissue adhesive hydrogel with tunable multifunctionality. *Bioactive Materials*. 2023;29:214–29. <https://doi.org/10.1016/j.bioactmat.2023.06.007>.
205. Li N, Li Y, Cheng Z, et al. Bioadhesive polymer semiconductors and transistors for intimate biointerfaces. *Science*. 2023;381:686. <https://doi.org/10.1126/science.adg8758>.
206. Lee HK, Yang YJ, Koirala GR, et al. From lab to wearables: innovations in multifunctional hydrogel chemistry for next-generation bioelectronic devices. *Biomaterials*. 2024;310:122632. <https://doi.org/10.1016/j.biomaterials.2024.122632>.
207. Zayats VV, Sergeev IK, Fedorov DA. Review of promising methods of supplying power to implantable medical devices. *Biomed Eng*. 2023;57:39–44. <https://doi.org/10.1007/s10527-023-10263-1>.
208. Jiang D, Shi B, Ouyang H, et al. Emerging implantable energy harvesters and self-powered implantable medical electronics. *ACS Nano*. 2020;14:6436–48. <https://doi.org/10.1021/acsnano.9b08268>.
209. Zhao X, Chen G, Zhou Y, et al. Giant magnetoelastic effect enabled stretchable sensor for self-powered biomonitoring. *ACS Nano*. 2022;16:6013–22. <https://doi.org/10.1021/acsnano.1c11350>.
210. Che Z, O'Donovan S, Xiao X, et al. Implantable triboelectric nanogenerators for self-powered cardiovascular healthcare. *Small*. 2023;19:2207600. <https://doi.org/10.1002/sml.202207600>.
211. Chan AYK. *Biomedical device technology: principles and design*, Third edition. Charles C Thomas, Publisher, Ltd, Springfield, Illinois
212. Yang SM, Shim JH, Cho H, et al. Hetero-integration of silicon nanomembranes with 2D materials for bioresorbable, wireless neurochemical system. *Adv Mater*. 2022;34:2108203. <https://doi.org/10.1002/adma.202108203>.
213. Roy S, Azad ANMW, Baidya S, et al. Powering solutions for biomedical sensors and implants inside the human body: a comprehensive review on energy harvesting units, energy storage, and wireless power transfer techniques. *IEEE Trans Power Electron*. 2022;37:12237–63. <https://doi.org/10.1109/TPEL.2022.3164890>.
214. Li S, Lu D, Li S, et al. Bioresorbable, wireless, passive sensors for continuous pH measurements and early detection of gastric leakage. *Sci Adv*. 2024;10:eadj0268. <https://doi.org/10.1126/sciadv.adj0268>.
215. Standard test method for rubber property—extension cycling fatigue. <https://www.astm.org/d4482-11r21.html>. Accessed 31 Aug 2024
216. 14:00–17:00. ISO 14708–1:2014. In: ISO. <https://www.iso.org/standard/52804.html>. Accessed 31 Aug 2024
217. Ruan Y, Robinson NB, Khan FM, et al. The translation of surgical animal models to human clinical research: A cross-sectional study. *Int Surg J*. 2020;77:25–9. <https://doi.org/10.1016/j.ijsu.2020.03.023>.

Publisher's Note Springer Nature remains neutral with regard to jurisdictional claims in published maps and institutional affiliations.

Authors and Affiliations

Xuan Li¹ · Xinghao Huang¹ · Liheng Yang² · Sunyoung Jung² · Jihe Wang³ · Hangbo Zhao^{1,2} 

✉ Hangbo Zhao
hangbozh@usc.edu

¹ Department of Aerospace and Mechanical Engineering, University of Southern California, Los Angeles, CA 90089, USA

² Alfred E. Mann Department of Biomedical Engineering, University of Southern California, Los Angeles, CA 90089, USA

³ Mork Family Department of Chemical Engineering and Materials Science, University of Southern California, Los Angeles, CA 90089, USA